Pergamon

Prog. Oceanog. Vol. 33, pp. 161-200, 1994

0079 - 6611/94 $26.00

0079-6611(94)00003-4

Outflows and deep water production by marginal seas

JAMES F. PRICE[1] and MOLLY O'NEIL BARINGER[1,2]

[1]*Woods Hole Oceanographic Institution, Woods Hole, MA, 02543, USA*
[2]*now at: Atlantic Oceanographic and Meteorological Laboratory, 4301 Rickenbacker Causeway, Miami, FL 33149, USA*

Abstract – We examine some of the processes that determine the properties of marginal sea outflows by reviewing historical data and by an analysis of two simple models. Our numerical simulation model makes several of the streamtube approximations of SMITH (1975), but goes on to include a Froude number-dependent entrainment parameterization, an Ekman number-dependent parameterization of broadening, and it can accept real bottom topography and real oceanic temperature and salinity profiles. This numerical model reproduces some of the main features of the four major outflows considered here (Mediterranean Sea, two from the Norwegian-Greenland Sea, and Weddell Sea) including the bulk properties of the product water.

A notable feature of these four outflows is that the density ordering of the source waters and product waters is reversed; for example, the densest source water comes from the Mediterranean Sea, and yet the Mediterranean outflow makes the least dense product water. The reason is that intense entrainment of North Atlantic Central Water decreases the density of the Mediterranean outflow by about 1kg m^{-3} as it begins to descend the continental slope. The three high-latitude outflows are more or less similar in that strong entrainment generally occurs over short segments of the path where the bottom topography is relatively steep, typically just beyond the shelf-slope break. However, the densities of these outflows are decreased much less by entrainment (about 0.1kg m^{-3} in the Denmark Strait outflow, about 0.2kg m^{-3} in the Faroe Bank Channel outflow and 0.03kg m^{-3} in the Weddell Sea outflow) as they descend to the bottom in their respective basins. Entrainment causes much less decrease in density in these outflows primarily because of the lower density differences between these outflows and their overlying oceanic waters. High latitude outflows are more likely to reach the bottom because the oceanic water column in polar and subpolar seas is weakly stratified. These and other results indicate that the temperature and salinity of the oceanic water column are of considerable importance in determining the product water of a marginal sea outflow.

Numerical experiments suggest that the density of the product water is remarkably insensitive to variations in the density of the source water. For example, if the density of the Mediterranean source water is arbitrarily increased by 1kg m^{-3}, then the increased density difference between outflow and overlying oceanic water results in even more vigorous entrainment. This increases the transport of product water by about $10^6 m^3 s^{-1}$ and limits the increase in density of the product water to only about 0.15kg m^{-3}. These and other results are obtained also from a simple end-point model of a descending outflow.

CONTENTS

1. DEEP WATER PRODUCTION BY MARGINAL SEAS

Most of the water that fills the deep sea has an origin in one of several marginal sea outflows (WARREN, 1981; LEE and ELLETT, 1965). In the present climate the densest water is produced in high latitude marginal seas and the deep ocean is filled with cold, polar waters. There are two important outflows in the Northern Hemisphere from the Norwegian-Greenland Sea – one through Denmark Strait, the other across the Iceland-Scotland Ridge and through the Faroe Bank Channel; there is at least one important outflow in the Southern Hemisphere from the Filchner Ice Shelf into the Weddell Sea and subsequently into the Southern Ocean. These northern and southern sources produce deep waters with roughly comparable densities, but with quite different chemical characteristics (BROECKER, 1991) and leave a distinctive imprint in deep sea sediments. Changes in chemical distributions over the deep North Atlantic around ten to twenty thousand years ago indicate that the northern hemisphere sources must have weakened during the glacial maximum (CURRY, DUPLESSEY, LABEYRIE and SHACKLETON, 1988; DUPLESSEY, SHACKLETON, FAIRBANKS, LABEYRIE, OPPO and KALLEL, 1988). Still further in the past, around fifty million years ago, the

deep water in the North Atlantic was much warmer and saltier than it is today (BRASS, SOUTHAM and PETERSON, 1982) and must have been produced mainly by evaporation over a subtropical shelf or marginal sea, perhaps something like the Mediterranean. With today's climate and continental configuration, the Mediterranean Sea produces a warm, salty source water that is very dense, and yet the end result of the modern Mediterranean outflow is an intermediate water mass. Why do some outflows produce bottom waters, while others (notably the Mediterranean outflow) do not? And how can tectonic or climatic changes over the marginal seas affect the product waters of their outflows?

In this paper we take up some aspects of the physical dynamics of marginal sea outflows by reviewing observations on the four major outflows noted above and by the development and analysis of two simple models. We hope to arrive at a partial synthesis of the observations and some understanding of how marginal sea outflows might change as part of a changing climate or changing earth.

1.1 Components of the deep water formation process

It is helpful to begin with an overview of the process of deep water formation by a marginal sea (Fig. 1) before launching into details. While no two cases are alike in every respect, all four of the major outflows have the following three components or steps in common:

(1) Air-sea exchange: Deep water is produced by outflows from marginal seas that are subject to either an unusually cold or an arid continental (rather than marine) climate. Intense and sustained air-sea exchange of heat or fresh water has to be sufficient to raise the density of the marginal sea waters, which become the 'source waters' of the outflows, to high values (potential density $\sigma_\theta \geq 28.0 \text{kg m}^{-3}$) at least intermittently (KILLWORTH, 1983).

(2) Ocean-sea exchange: These marginal seas are distinguished by being semi-enclosed both horizontally and vertically so that they have a restricted exchange of water with the open ocean. Thus these semi-enclosed marginal seas are concentration basins that produce a smaller volume of denser water than would be produced in an open ocean site subject to the same air-sea exchange. In two of the cases noted (Mediterranean and Faroe Bank Channel), the exchange rate appears to be determined by hydraulic control phenomena and is dependent upon the density contrast between the marginal sea and the open ocean, and upon the width and depth of the constriction (BRYDEN and STOMMEL, 1984; WHITEHEAD, 1988; BRYDEN and KINDER, 1991; PRATT and LUNDBERG, 1991). In the other two cases (Weddell Sea and Denmark Strait), the exchange process is more complex, and may include a contribution from the basin scale circulation.

(3) Descent and entrainment: Before the dense source waters can reach the open ocean they must descend the continental shelf and slope (WHITEHEAD, 1989). As the outflows descend into the open ocean they entrain a substantial volume of the overlying oceanic water (LEE and ELLETT, 1965; SMITH, 1975), typically doubling their initial volume transport. Because of this entrainment, the resulting 'product waters' that finally settle into the open ocean (and which are named water types) may have quite different characteristics from the source waters which first outflowed from the marginal sea.

Most previous studies of deep water formation have emphasized the first and second steps of the process (SWIFT and AAGAARD, 1981; BRYDEN and STOMMEL, 1984). The first step, air-sea exchange, is the connection between the atmosphere and the deep ocean, and is subject to change with varying climate or ice cover. The second step, ocean-sea exchange, may vary if the density contrast with the open ocean changes for any reason, or if the configuration of the strait or sill changes. Taken together, these first two steps determine the heat and salt budget of the marginal sea and thereby the Θ-S properties of the source waters of the outflows.

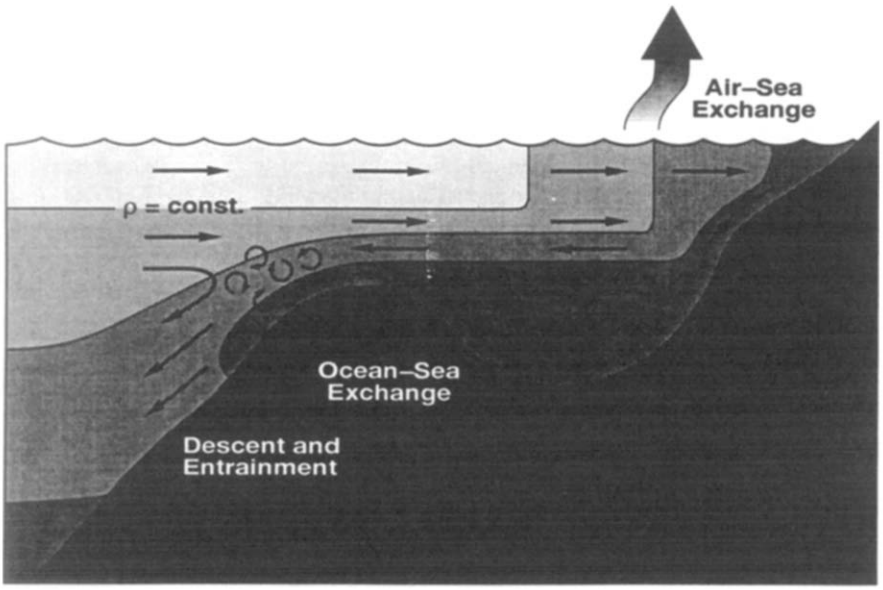

FIG. 1. A schematic of deep water formation by a marginal sea. This schematic is closest in detail to the Mediterranean case in that it shows a two-layer ocean-sea exchange and a product water that settles into the open ocean at mid-depths. All of the other outflows produce a bottom water type, and the Denmark Strait and Weddell Sea cases do not appear to have a simple, two-layer, ocean-sea exchange. We have also indicated an outflow of dense water from the shelf into the deep basin of the marginal sea; the process of deep water formation within a marginal sea (LACOMBE, 1990) can be similar to the process of deep water formation by a marginal sea that is the topic here. These three components of the deep water production process are also the successive steps in the transformation of marginal sea surface water into oceanic deep water. The air-sea interaction step that begins the process is thought to be highly seasonal, at least in the Mediterranean and Norwegian-Greenland Seas. Nevertheless, the four major outflows are observed to be fairly steady on seasonal time scales (Mediterranean, BRYDEN and KINDER, 1991; Denmark Strait, DICKSON, GMITROWICZ and WATSON, 1990; Faroe Bank Channel, SAUNDERS, 1990; Filchner Ice Shelf, FOLDVIK, KVINGE and TORRESEN, 1985c).

1.2 The density ordering of source waters and product waters

The third step in the deep water formation process is also of some importance as evidenced by a surprising relationship of source waters to product waters. Namely, the density ordering of the source waters is just the reverse of the density ordering of product waters. A listing of the source waters in order of increasing potential density is:

(1) Filchner Ice Shelf Water, $\sigma_\theta = 27.93 \text{kg m}^{-3}$, which is the least dense by virtue of its low salinity;
(2) Denmark Strait source water, which is mainly Arctic Intermediate Water, $\sigma_\theta = 28.04 \text{kg m}^{-3}$;
(3) Faroe Bank Channel source water, which is mainly Norwegian Sea Deep Water, $\sigma_\theta = 28.07 \text{kg m}^{-3}$; and
(4) Mediterranean source water, which is mainly Levantine Intermediate Water[1], and is the densest by virtue of its high salinity, $\sigma_\theta = 28.95 \text{kg m}^{-3}$.

[1]STOMMEL, BRYDEN and MANGELSDORF (1973) and BRYDEN and STOMMEL (1982) found that the Mediterranean source water is made up of two different water types. The largest volume is Levantine Intermediate Water having Θ = 13.10°C and S = 38.47, and there is a smaller volume of Western Mediterranean Deep Water having Θ = 12.78°C and S = 38.43. For the present purpose it is sufficient to ascribe a single, average value to Mediterranean source water, Θ = 13.0°C and S = 38.45, and arrive at the density listed.

After these source waters have gone through their respective outflows and have settled into the open ocean, their density ordering is just reversed from that above. A listing of the product waters in order of increasing density, and indicating density at 4000m as σ_4 is:

(1) Mixed Mediterranean water, which makes an intermediate water mass in the North Atlantic thermocline, $\sigma_\theta = 27.70 \text{kg m}^{-3}$ and $\sigma_4 = 44.91 \text{kg m}^{-3}$
(2) North East Atlantic Deep Water (also called Gibbs Fracture Zone Water) produced by the Faroe Bank Channel outflow, $\sigma_\theta = 27.90 \text{kg m}^{-3}$ and $\sigma_4 = 45.88 \text{kg m}^{-3}$
(3) North West Atlantic Deep Water produced by the Denmark Strait outflow, $\sigma_\theta = 27.92 \text{kg m}^{-3}$, $\sigma_4 = 46.07 \text{kg m}^{-3}$; and finally the densest product water of the four is
(4) Weddell Sea Bottom water resulting from the Filchner Ice Shelf outflow, $\sigma_\theta = 27.89 \text{kg m}^{-3}$, $\sigma_4 = 46.20 \text{kg m}^{-3}$. (This product water is the densest when *in situ* densities are compared at depths greater than about 1km.)

This reordering indiates that mixing (or entrainment) must vary significantly between these four outflows and is evidently a crucial part of the overall process that produces deep water. Our main goal here is to develop some understanding of this mixing process, and specifically to learn how the product water of an outflow depends upon its source water properties, and upon the oceanic conditions it encountered along its path. An appropriate test of our understanding is to address the question: Why do the four major outflows exhibit density reordering?

1.3 Localized mixing

A subtle but important characteristic of this mixing process is that it is quite variable in intensity along the path of an outflow. This has been described in some detail for the Mediterranean outflow (PRICE, O'NEIL BARINGER, LUECK, JOHNSON, AMBAR, PARILLA, CANTOS, KENNELLY and SANFORD, 1993) and is evident in the historical data on some of the other outflows. The density of the Denmark Strait outflow decreases by about 0.1kg m^{-3} within the first several hundred kilometers of its descent into the Irminger Sea (SMITH, 1975), so that the spatial rate of change of density is $O(10^{-6} \text{kg m}^{-2})$ over the first portion of the path. This outflow continues on around Cape Farewell and southward along the continental slope of North America as part of the deep core of the Deep Western Boundary Current (DWBC) (SWIFT, 1984a; PICKART, 1992). Beyond Cape Farewell this outflow shows a much reduced rate of change of density, $O(10^{-8} \text{kg m}^{-2})$, and endures for many thousands of kilometres (SPEER and MCCARTNEY, 1991; SMETHIE, 1993). The strong mixing process that determines the conversion of source water to product water is thus quite localized, and as will be shown later, is closely tied to the bottom topography. In this telling respect, this strong mixing process is quite different from the homogeneous diffusion process that is usually considered to modify the properties of large scale ocean currents (e.g. REID and LYNN, 1971, describe the gradual evolution of product waters as they circulate through the world ocean). A second appropriate test of our understanding of outflows is then: Why is intense mixing localized?

1.4 The plan

The main contribution of this paper is a simple numerical simulation model introduced in Section 2.1 and an even simpler analytic model given in Section 2.2.3 (readers who are more interested in outflows than in models are urged to try at least the latter). The Mediterranean and Denmark Strait outflows are considered in the most detail in Sections 3 and 4.1. The Faroe Bank Channel and the Filchner Ice Shelf outflows are taken up in somewhat less detail in Sections 4.2 and 5. The main results are summarized in Section 6, where we also attempt a quantitative accounting of density reordering.

2. DENSITY CURRENT MODELS OF OUTFLOWS

The starting point for both the models used here is the assumption that outflows are density-driven bottom currents, and that the strong mixing process, highlighted in Section 1, is an entrainment process that is an integral part of the density current dynamics. This view was developed in an experimental laboratory context by ELLISON and TURNER (1959), and was first applied to an oceanic outflow by CREASE (1965). It was the basis of the first outflow model developed by SMITH (1975) whose work we build upon here. (Surveys of density currents are given by TURNER, 1973, and SIMPSON, 1987.)

2.1 A one-dimensional numerical model

A second assumption is that the outflow can be represented by a single layer having a height H and width W (Fig.2) that can vary separately. The geometry of this model is otherwise similar to that of the streamtube models of SMITH (1975) and KILLWORTH (1977).

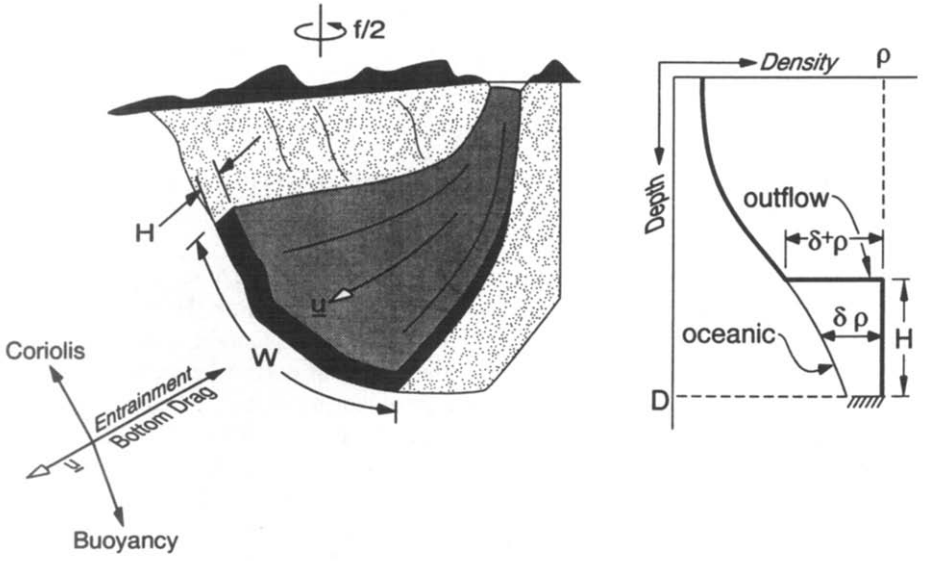

FIG.2. A schematic of the model outflow and density profile. Marginal sea outflows are thin, having aspect ratios H/W in the range 0.01 to 0.001, and are fairly broad in the sense that $W/x \approx 0.3$ well downstream from the start, where x is the distance downstream. They are also broad in the sense that $\alpha W > H$ at distances well downstream from the start, where α is the bottom slope.

A third assumption is that the outflow is steady, so that the only independent variable is the along-stream distance. The numerical model is thus one-dimensional. A model having this highly simplified geometry may be useful for examining the bulk (across-stream and depth-averaged) changes in properties along the path of the outflow, which is our main interest here. However, it clearly can not give insight into the boundary layer structure or the horizontal structure of a real outflow (some discussion of which is in PRICE, O'NEIL BARINGER, LUECK, JOHNSON, AMBAR, PARILLA, CANTOS, KENNELLY and SANFORD, 1993, and JOHNSON and SANFORD, 1992a). The steady assumption is probably valid for seasonal and longer time scales as noted in Section 1. It is not at all clear if shorter period fluctuations can be safely ignored, but these are beyond the scope of the present model (more on this in Section 4.1.2).

A fourth assumption is that the oceanic environment is effectively infinite and is at rest. Thus the oceanic environment is specified by temperature and salinity profiles $\Theta_{ocn}(z)$ and $S_{ocn}(z)$, that are presumed given. By taking the oceanic environment to be a given, the dynamics of the outflow are assumed to be completely separated from the dynamics of the surrounding ocean. This may be appropriate for a study of the local dynamics of an outflow if the density-driven currents within the outflow are much larger than the currents in the overlying ocean. This appears to hold true at locations downstream of the sill (in the Mediterranean outflow it holds within the Gulf of Cadiz, but not within the Strait of Gibraltar proper).

2.1.1. Budgets and parameterizations. The momentum conservation equation for the outflow layer is written,

$$\mathbf{U}\cdot\nabla\mathbf{U} + \mathbf{f}\times\mathbf{U} = g\delta\rho\nabla D/\rho_r - \tau_b/\rho_r H - EU/H \qquad (1)$$

where $\mathbf{U}$ is the horizontal current, $\mathbf{f}$ is the Coriolis parameter times the vertical unit vector (f is taken as constant), and ρ_r is a constant reference density. The density difference between the outflow and the oceanic water is taken to be the density difference at mid-depth in the outflow, $\delta\rho = \rho - \rho_{ocn}(D-H/2)$ when computing the average buoyancy, while the density difference relevant for estimating entrainment is taken to be the density difference at the top of the outflow, $\delta^+\rho = \rho - \rho_{ocn}(D-H)$ (Fig.2) (outflow variables are unsubscripted). In either case it is important to take account of pressure effects upon the density difference (LYNN and REID, 1968; REID and LYNN, 1971; KILLWORTH, 1977) which is therefore computed from *in situ* density using EOS80 as the state equation.

An important simplification of a streamtube model is that the outflow is assumed to be thin enough for the baroclinic pressure gradient term arising from the along-stream variation of column height or density to be small compared to the buoyancy acceleration resulting from the density difference and bottom slope, i.e.

$$\nabla(\delta\rho H^2/2) << H\delta\rho\nabla D, \qquad (2)$$

where ∇ is the horizontal gradient operator, and D is the bottom depth. By omitting the baroclinic pressure term, the model dynamics are reduced to those of a density-driven bottom current over sloping topography; a model made with this approximation can not be initialized upstream of a major sill (for example in the western Mediterranean Sea east of Gibraltar). This approximation can be checked later for consistency, and is well satisfied on average in these solutions. Nevertheless there are places where the baroclinic pressure gradient may be important locally (flow over bumps, and possibly near the sill of the Faroe Bank Channel outflow, more on this in Section 4.2).

The stress on the ocean bottom, τ_b, is parameterized by the usual quadratic form, $\tau_b = \rho_r C_d UU$, where the drag coefficient is assumed to have the nominal, constant value $C_d = 3\times10^{-3}$. JOHNSON AND SANFORD (1992b) deduced a roughly similar value from an analysis of data from the Mediterranean outflow. We suspect that this C_d is uncertain to probably 50% for any specific portion of an outflow path. For example, field studies of the atmospheric boundary layer (STULL, 1988) suggest that C_d likely depends upon the roughness Reynolds number, whose variation is unknown and thus ignored here.

The last term in Eq.1 is the entrainment stress term, where the entrainment rate, E, is a positive definite velocity that is parameterized as a function of the layer Richardson number, $R = g\delta\rho^+ H/\rho_r U^2$. Based upon laboratory experiments by ELLISON and TURNER (1959) and subsequent analysis (TURNER, 1986), the function is taken to be

$$\left.\begin{aligned} &E = U(0.08 - 0.1R)/(1+5R) \text{ if } R \le 0.8, \text{ and} \\ &E = 0 \text{ otherwise.} \end{aligned}\right\} \qquad (3)$$

In most later discussions the internal Froude number, $F = R^{-1/2}$, is used in place of the Richardson number. CREASE (1965) and SMITH (1975) both suggested that an entrainment parameterization of this form should be appropriate for outflows, and STURGES (1975) found that the internal Froude number of an overflow from the North Atlantic into the Caribbean Sea was near 1. The essential feature of this parameterization is that it couples entrainment to the dynamics of the current. Entrainment becomes significant when F exceeds about 1 (or R is below 1), which in practice happens where the current is accelerated by steep topography. Entrainment is otherwise vanishingly small. This kind of parameterization yields solutions having a very pronounced along-stream intermittence of mixing, which appears to be an important feature of real outflows.

Heat and salt conservation equations for the outflow are just

$$\left.\begin{aligned} \mathbf{U}\cdot\nabla\Theta &= -E\delta^{+}\Theta/H \\ \mathbf{U}\cdot\nabla S &= -E\delta^{+}S/H \end{aligned}\right\} \tag{4}$$

where the only way in which Θ, S or potential density can change is by entraining or mixing with the overlying water (entraining and mixing are used interchangeably; in a single-layered model such as this one the only mixing is by entrainment). As noted above, the buoyancy of the outflow is computed from the *in situ* density difference, $\delta\rho = \rho(S,\Theta,P) - \rho_{ocn}(S_{ocn}(P), \Theta_{ocn}(P),P)$. Thus the *in situ* density difference can change along the path by three different processes (and using d/dt in lieu of the advection operator above),

$$\frac{d\delta\rho}{dt} = \frac{\partial\rho}{\partial\Theta}\frac{d\Theta}{dt} + \frac{\partial\rho}{\partial S}\frac{dS}{dt} - \frac{dP}{dt}\left(\frac{\partial\Theta_{ocn}}{\partial P}\frac{\partial\rho_{ocn}}{\partial\Theta} + \frac{\partial S_{ocn}}{\partial P}\frac{\partial\rho_{ocn}}{\partial S}\right) + \frac{dP}{dt}\left(\frac{\partial\rho}{\partial P} - \frac{\partial\rho_{ocn}}{\partial P}\right) \tag{5}$$

The first two terms represent the effect of entrainment (Eq.4), and always act to reduce the density difference. The third term represents the effects of descent into a stratified oceanic water column, which also acts to reduce the density difference. The fourth term represents the thermobaric effect (KILLWORTH, 1977) which can either increase or decrease the density difference depending upon the difference in compressibilities; cold sea water is more compressible than warm sea water, and hence a cold outflow will acquire an enhanced *in situ* density difference as it descends into a warmer oceanic environment. Some of the diagnostics shown later use the potential density of the outflow, or the potential density difference, rather than the *in situ* density difference. From Eq.5 it is evident that the potential density of the outflow can be changed only by entrainment and that the potential density difference can be changed by entrainment and descent.

Finally, the continuity equation for the outflow is taken to be

$$\mathbf{U}\cdot\nabla H = E - H\mathbf{U}\cdot\nabla W/W - H\nabla\cdot\mathbf{U} \tag{6}$$

where the rate of increase of the width is specified by

$$(\mathbf{U}\cdot\nabla W)/U = \beta, \tag{7}$$

where β can be specified *a priori* if the outflow width is constrained by a channel (which happens in the Mediterranean case). Otherwise, broadening obviously involves the transverse velocity component and has to be parameterized in a one-dimensional model such as this one. As a start, GRIFFITHS (1986) showed that an inviscid outflow, once geostrophically adjusted to a constant slope, will neither descend nor broaden as it moves downstream (though variations of buoyancy

or bottom slope could cause changes in width and depth as shown by BARINGER, 1993). This suggests that bottom drag could be an important element of broadening, and leads to a first guess at a parameterization,

$$\beta = 2K, \tag{8}$$

where $K = (\tau_b/\rho_r H)/(fU)$ is the Ekman number, the ratio of bottom drag to the Coriolis acceleration. The factor 2 comes from combining the observation that the upslope side of an outflow descends topography only very slowly compared with the downslope side (e.g. see AMBAR and HOWE, 1979b, and MANN, 1969), and from the model result that the outflow as a whole descends across isobaths at an angle $U_{across}/U_{along} = K$, where U_{across} and U_{along} refer to the current components across and parallel to the isobaths. The outflow width should thus increase with distance downstream at about twice that rate (or a little less, but the leading constant is rounded off to avoid any suggestion of high precision). This parameterization is found to give reasonable results, and moreover the solutions for outflow temperature, salinity and density are not particularly sensitive to the details of broadening. In that respect the parameterization (Eq.8) is acceptable for now, but we caution that it does not describe time-dependent broadening and may underestimate the width in a case in which the initial width is comparable to the radius of deformation (which may be important in the Faroe Bank Channel case, Section 4.2).

2.1.2. Implementation. These model equations can be readily integrated numerically because Eq.1 and Eq.2 assure that information propagates downstream only. Thus the equations can be stepped forward in time from the initial condition, which is the starting position of the outflow and the initial values of Θ, S, **U**, H, and W (the model analogues of the source water properties) by following a single column that flows over the bottom topography subject to the accelerations modelled by Eq.1. Since the outflow is assumed to be in steady state, the temporal changes computed following a single column are kinematically equivalent to the spatial rate of change that appears in the Eulerian balances.

In the first numerical experiments, the bottom topography was represented by a plane. It soon became apparent that the bottom slope is a crucially important external parameter (described further below) and inspection of topographic charts showed that bottom slope varies substantially along the paths of most of the outflows. Bottom topography is, therefore, taken from a digital data base, DBDB5, that has a horizontal resolution of 5 minutes of latitude and longitude. To estimate the bottom slope, a centered spatial difference is taken over the width of the outflow. This gives a somewhat smoothed representation of the bottom topography; such smoothing is not required for numerical stability and has very little effect on the final results.

2.1.3. Expectations. Although we have called this a 'simulation' model, since important observed data (oceanic hydrography, bottom depth and initial conditions of the outflow) are inserted for each case, it is by no means a comprehensive simulation model. Rather, the model physics have been pared down to the absolute minimum that might possibly suffice for the problem posed. In particular, there is no driving force other than the outflow's own buoyancy, and there is only one mixing process recognized in the model. In this regard the model might better be termed a narrowly defined 'process' model.

The absolute accuracy of the model is consequently very hard to define *a priori*, and even the uncertainty of specific parameterizations is hard to define objectively since the plausible range of an entrainment parameterization or the uncertainty of the bottom drag coefficient is a highly subjective call. Perhaps the best test of such a model is a pragmatic one made *a posteriori*, namely, whether the model can simulate all four cases well enough to clearly distinguish the differences among them. Perhaps it is fortunate that in the four cases considered here, the parameter range is

large enough for the model to achieve this to some degree (though one important feature of the Faroe Bank Channel simulation points to a missing mixing or dynamical process). To the extent that the model can distinguish among these four cases, it makes a credible tool for analysis of outflow dynamics, and for estimating the sensitivity of the outflows to variations of geophysical variables such as the initial or oceanic conditions.

2.2 Some special cases

The model dynamics includes several very simple limiting cases that are worth examining briefly before going on to the simulations of natural cases (see also SMITH, 1975, and GRIFFITHS, 1986).

2.2.1. A non-entraining density current. To illustrate the effects of bottom friction and rotation, consider a case in which the entrainment is set to zero, so that there is no entrainment drag and no change in outflow density. Assume that the environment has a constant density, so that the density difference between the outflow and the environment is also constant. The width is also held fixed, but the column height can change by stretching if the column accelerates, i.e. the continuity equation becomes just $UH = Q$ = constant, where Q is the source strength (volume flux) per unit width. The column is allowed to slide down a planar slope having a magnitude α, and a bottom drag coefficient C_d, which can be imagined to vary from case to case. The character of the motion is then determined by the initial condition, and by the Ekman number. In the frictionless limit, $C_d = 0$, the motion is that of a cycloid; a column accelerates downslope for half of an inertial period until it is turned by rotation. The column acquires a mean motion that is along a bottom contour and is geostrophic, while retaining an inertial oscillation. A peculiarity of a streamtube model of this sort is that if the current vanishes, then the layer thickness must become infinite in order to conserve Q. This is (much) better avoided in simulations of real cases by choosing an initial condition that is not too far from a geostrophic balance.

If C_d is nonzero, then the inertial motion is damped at a rate C_dU/H, and the time-averaged current descends across isobaths at an angle K as noted earlier. Assuming that the speed is the geostrophic speed, $U \approx g'\alpha/f$, where $g' = g\delta\rho/\rho_r$ is the reduced gravity and α is the bottom slope, then a geostrophic Ekman number can be written in terms of external variables as

$$K_{geo} = \frac{C_d g'\alpha}{Hf^2} = \frac{C_d(g'\alpha)^2}{Qf^3} \tag{9}$$

The Ekman number of the outflows is generally in the range $K_{geo} \leq 0.2$ so that a slightly damped, nearly geostrophic balance characterizes most of the path (most of the distance) along all of the outflows. Bottom drag is nevertheless crucial in that it allows an outflow to descend topography without necessarily accelerating. A second important effect of bottom drag was alluded to above, namely, that bottom drag causes or allows an outflow to broaden as it moves downstream.

2.2.2. An entraining channel flow. A second special case is that of a steady channel flow (no rotation) that is subject to bottom stress and entrainment (i.e. ELLISON and TURNER, 1959; PRATT, 1986). The momentum budget can be written

$$g'\alpha = C_d \frac{U^2}{H} + \frac{EU}{H} \tag{10}$$

where U is the current amplitude and recall that E is positive definite. If the buoyancy acceleration is balanced by the bottom stress, then E = 0. If the buoyancy force exceeds the bottom stress, then the entrainment stress (or interfacial stress) also contributes to balancing the buoyancy force, and by minor rearranging the normalized entrainment velocity can be written as the difference between buoyancy and drag as

$$\frac{E}{U} = \alpha R - C_d. \tag{11}$$

The essential thing is then to know under what conditions entrainment will occur. If entrainment occurs when R = 1 or less, then no entrainment will occur unless $\alpha \geq C_d$ (recall that the baroclinic pressure gradient is neglected in this). If $C_d \approx 3 \times 10^{-3}$, then bottom stress should be sufficient to balance the entire buoyancy force on a continental shelf but not on a continental slope. This is the first hint that the shelf-slope break is likely to be a crucial region for outflows (though rotation is important too, of course).

Assuming that R is near 1, and defining an equivalent friction velocity to be $u_* = \sqrt{g'H(\alpha - C_d)}$, then the momentum budget can be rearranged a little further to solve for another nondimensional entrainment rate in terms of an external Richardson number, $R_* = g'H/u_*^2$,

$$\frac{E}{u_*} \approx R_*^{-1/2}, \tag{12}$$

which is found in laboratory studies of quasi-steady entrainment (PRICE, 1979; TURNER, 1986). This remarkably simple result is parameter free (though R = 1 is implicit if this is the model result), and it has an appealing physical interpretation that is not apparent in the more complex empirical form (Eq.3). It indicates that if the Richardson number reaches its critical value, entrainment then occurs at a rate that is proportional to the amplitude of the forcing, in this case topographic acceleration less bottom stress. This can be used in the simulations in lieu of Eq.3 and gives results that are nearly indistinguishable, provided that the outflow is slowly varying in the Lagrangian frame (not true in the Mediterranean case).

From the two special cases above it appears that bottom stress, though clearly important, is not a leading term in the momentum balance. This suggests some further simplifications that lead to a third special case, an entraining density current with rotation, that is important enough to take up in some detail.

2.2.3. Entraining density currents with rotation; an end-point model of an outflow. By making three further approximations on the budget equations of the numerical model we can arrive at a very simple solution for the final state of an outflow that anticipates most of the parameter dependence found in the numerical simulations. This is dubbed an 'end-point' model to distinguish it from the one-dimensional numerical model and to emphasize that it gives the final or product water properties only. The first two of these approximations may appear plausible *a priori*, though the third approximation requires support from the numerical model and field observations presented in the next three sections. This simplest of all outflow models is made as follows:

(1) The currents in most outflows are nearly geostrophic, and the current speed, U, can be approximated by the geostrophic speed, $U_{geo} = g'\alpha/f$, where g' will change (be reduced) if there is entrainment.

(2) Bottom stress is small enough for its effect upon the current speed to be ignored (repeats 1 above), but the bottom stress effect upon width is retained so that

$$W(x) = W_{src} + 2K_{geo}x, \tag{13}$$

where W_{src} is the initial width just over the sill, K_{geo} is the geostrophic Ekman number ($\approx$0.2 for most cases), and x is the distance downstream from the start. The continuity equation then gives the column height, in the absence of entrainment, as

$$H_{geo} = H_{src}U_{src}/U_{geo}(1 + 2K_{geo}x/W_{src}). \tag{14}$$

A geostrophic Froude number can be defined from the geostrophic speed and this 'geostrophic' column height,

$$F_{geo} = \frac{U_{geo}}{\sqrt{H_{geo}g'_{src}}} \tag{15}$$

where g'_{src} is based upon the initial density difference. It is also useful to define a buoyancy flux per unit width of the outflow,

$$B = HUg', \tag{16}$$

and the geostrophic version,

$$B_{geo} = H_{geo}U_{geo}g'_{src} = H_{src}U_{src}g'_{src}/(1+2K_{geo}x/W_{src}). \tag{17}$$

Note that B will decrease with distance downstream if the outflow current becomes wider.

(3) Results in later sections show that strong entrainment is generally localized to a region just downstream of the shelf-slope break where F first exceeds 1, which is therefore taken as a hard upper limit on the actual Froude number (i.e. entrainment is assumed to occur at a rate that keeps the actual Froude number from exceeding 1). Since the site of the entrainment is fairly shallow and localized in depth, this mixing is termed an 'entrainment event', and the variation of stratification over the depth range of the entrainment event can be ignored.

Under these approximations, the product water density of an outflow is just

$$\rho_{prd} = \rho_{src} \text{ if } F_{geo} \leq 1, \tag{18}$$

i.e. if E = 0 and there is no entrainment, or,

$$\rho_{prd} = \rho_{src} - (\rho_{src} - \rho_{ocn})(1 - B_{geo}^{1/3}/U_{geo}) \text{ if } F_{geo} \geq 1, \tag{19}$$

in which case there is entrainment. B_{geo} and U_{geo} are evaluated at the entrainment site where $x = X_e$, and $\alpha = \alpha_{max}$. In most cases Eq.19 will hold because

$$F_{geo} = \frac{(g(\rho_{src} - \rho_{ocn})/\rho_r)(\alpha_{max}/f)^{3/2}}{(H_{src}U_{src}/(1 + 2K_{geo}X/W_{src}))^{1/2}} \geq 1, \tag{20}$$

is likely to be satisfied somewhere along the path of an outflow. For example, if $f = 10^{-4} s^{-1}$, $U_{src} = 0.5 m\, s^{-1}$, $H_{src} = 100m$, and $\rho_{src} - \rho_{ocn} = 0.5 kg\, m^{-3}$, then Eq.19 would be satisfied for $\alpha_{max} \geq 9 \times 10^{-3}$, which is exceeded on most continental slopes (all of the outflows begin on a continental shelf and have to cross the continental slope before reaching the open ocean).

The factor

$$\Phi = 1 - B_{geo}^{1/3}/U_{geo} = 1 - F_{geo}^{-2/3} \tag{21}$$

appearing in Eq.19 is a direct measure of how much entrainment occurs; $\Phi = 0$ indicating no entrainment whatever so that $\rho_{prd} = \rho_{src}$ (same as Eq.18), while $\Phi \rightarrow 1$ indicates that entrainment is extremely large, and that $\rho_{prd} \rightarrow \rho_{ocn}$. The temperature, salinity and transport of the product water can be written in terms of Φ and the source and oceanic values as:

$$T_{prd} = T_{src} - (T_{src} - T_{ocn})\Phi, \tag{22}$$

$$S_{prd} = S_{src} - (S_{src} - S_{ocn})\Phi, \tag{23}$$

and,

$$M_{prd} = M_{src} \frac{1}{1-\Phi}. \tag{24}$$

Note that the normalized change in density or temperature and salinity is also equal to Φ, i.e.

$$\frac{\rho_{src} - \rho_{prd}}{\rho_{src} - \rho_{ocn}} = \frac{\Delta\rho}{\delta\rho_{src}} = \Phi, \tag{25}$$

all of which make clear that the key to understanding this model is to know how Φ depends upon the external variables. From Eq.20 and Eq.21 one can see that Φ will be increased (there will be more entrainment) if (1) B_{geo} is decreased, which would occur if the initial transport per unit width were decreased or if the outflow width increased, or if (2) U_{geo} is increased, which would occur if the density difference or the bottom slope were increased. This latter dependence is likely to be the more important along the path of any specific outflow, however the case-to-case variation of B is also important when comparing the outflows.

An alternative expression for the product density can be derived by rearranging Eq.19:

$$\rho_{prd} = \rho_{ocn} + \frac{\rho_r B_{geo}^{1/3}}{g\alpha_{max}/f} = \rho_{ocn} + \delta\rho_{src}(1-\Phi), \tag{26}$$

which shows that the only relevant flow parameter is B_{geo}, which is conserved under entrainment. Thus, the product density is not affected by entrainment that may precede the so-called entrainment 'event' and which is, of course, distributed over some finite portion of the path. A second interpretation of the entrainment effect upon outflow density is suggested by Eq.26 which shows that the density difference of the outflow after the entrainment event is just $\delta\rho_{src}(1-\Phi)$. That is,

unless $\Phi = 1$, which never quite happens, then the outflow will retain some density difference with respect to the oceanic water. Whether this remaining density difference is sufficient to cause the outflow to sink all the way to the bottom then depends upon (1) the stratification of the oceanic water column below the depth of the entrainment event and (2) the effects of compressibility, which can be substantial if the outflow density difference results in part from a temperature difference (recall Eq.5).

The end point solution for product density is plotted in Fig.3 to show the dependence upon source density and oceanic density. The solid curve shows the effect of varying the source density while holding the oceanic density (and all else) constant, while the dashed curve shows the effect of varying the oceanic density while holding the source density constant. For the parameters chosen (see caption), $F_{geo} < 1$ if the density difference is less than about 0.4kg m^{-3}. In that parameter range there is no mixing, and so the product density equals the source density; the solid curve increases like ρ_{src} while the dashed curve is constant at the initial value. As the density difference exceeds 0.4kg m^{-3} and entrainment occurs, the solid curve begins to fall off to approximately $\delta\rho_{src}^{1/3}$, showing a weak dependence of product density upon source density. The derivative of the solution for product density is just

$$\partial\rho_{prd}/\partial\rho_{src} = \frac{1 - \Phi}{3} \tag{27}$$

which shows that the sensitivity is reduced to zero as Φ approaches 1 ($\Phi \approx 1/2$ for the four major outflows).

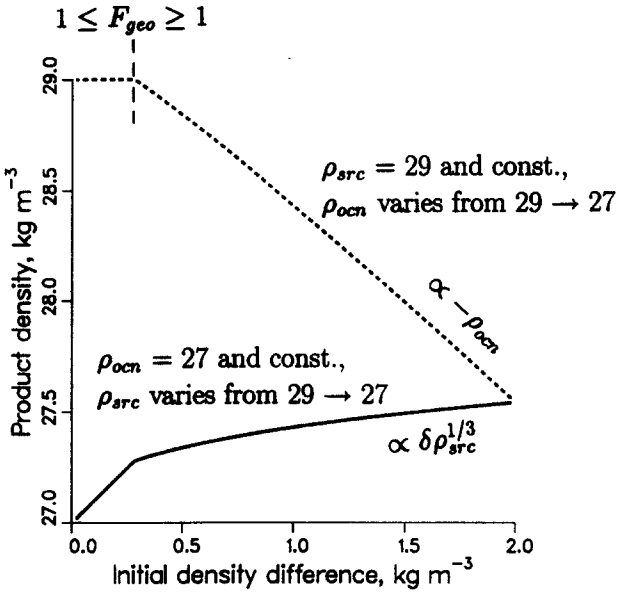

FIG.3. Product water density of an outflow shown as a function of the initial density difference. The dashed curve results from varying the oceanic density while holding the source density constant at 29kg m^{-3}; the solid curve results from varying the source density while holding the oceanic density constant at 27kg m^{-3}. The other conditions are meant to be nominal: $f = 10^{-4}$s^{-1}, $U_{src} = 1.0$m s^{-1}, $H_{src} = 100$m, and $\alpha = 20 \times 10^{-3}$.

This weak dependence of ρ_{prd} upon ρ_{src} is a striking feature of the numerical model results described in later sections. To understand this qualitatively, imagine that the source density of an outflow is arbitrarily increased. The increased source density will cause an increase in the density difference, which in turn will cause larger geostrophic currents, larger Φ, and thus larger entrainment. Since the density difference is increased, the effect of the entrainment in reducing the density of the outflow is increased substantially, sufficient to wipe out most of the imposed increase of the source density. Thus the dynamics of the entrainment process provide a very strong damping on variations of the source density. The same qualitative result, though with greater or lesser sensitivity, would occur in other outflow models in which the entrainment increased with current speed (SMITH, 1975; KILLWORTH, 1977).

A surprising result is that the product density of an outflow is considerably more sensitive to variations of the oceanic density,

$$\partial\rho_{prd}/\partial\rho_{ocn} = \frac{2+\Phi}{3} \tag{28}$$

(and see Fig.3). This too can be understood in a qualitative way by retracing the steps following Eq.27. Note that Eq.27 and Eq.29 have the same sign indicating that an increase in either the source density or the oceanic density will cause an increase in the product density of an outflow (though the sensitivity is quite different as noted above). It might have been expected that variations of the source and oceanic densities would be in some way equivalent or symmetric in their effect upon product density. However, the entrainment process is inherently asymmetric in that only the outflow density is affected by entrainment, and can only be decreased by entrainment.

The product water density is emphasized in the following discussion because density (or Φ-S) is the easiest outflow property to observe in the ocean. The models also give an estimate of the product water transport. For example, an increase of the source water density causes an increase of entrainment and consequently an increase in the product water transport that goes as

$$\frac{\delta\rho_{src}}{M_{src}}\frac{\partial M_{prd}}{\partial\rho_{src}} = \frac{2/3}{1-\Phi} \tag{29}$$

Similarly, the product water transport varies with ρ_{ocn} as

$$\frac{\delta\rho_{src}}{M_{src}}\frac{\partial M_{prd}}{\partial\rho_{ocn}} = \frac{-2/3}{1-\Phi} \tag{30}$$

which is the same, except for the sign. These both indicate a marked sensitivity of the product water transport to variations of source or oceanic density (just the complement of Eq.27 in the sense that $(\partial/\partial\rho_{src})(\delta\rho_{src}M_{src}) = (\partial/\partial\rho_{src})(\delta\rho_{prd}M_{prd})$). This is likely to be of some importance to the thermohaline circulation.

3. THE MEDITERRANEAN OUTFLOW

Evaporation over the Mediterranean basin produces a highly saline source water, S = 38.4, that is very dense, $\sigma_{\theta src} = 28.95 kg\ m^{-3}$. Its density exceeds that of North Atlantic bottom water, $\sigma_\theta \approx 27.9 kg\ m^{-3}$, and greatly exceeds the density of the surface water found just outside the Mediterranean. This results in a horizontal density contrast that drives an inverse estuarine circulation through the shallow and narrow Strait of Gibraltar. Relatively fresh and warm Atlantic surface water forms an inflowing upper layer that is transformed by evaporation into saltier, cooler and much denser Mediterranean deep water that forms an outflowing layer (BRYDEN and STOMMEL, 1984; ARMI and FARMER, 1988; BRYDEN, CANDELA and KINDER, 1994). The dense Mediterranean water spills over the shallow sills in the Strait of Gibraltar and cascades down the continental shelf and slope into the Gulf of Cadiz and on into the open North Atlantic (HEEZEN and JOHNSON, 1969; AMBAR and HOWE, 1979a,b; HOWE, 1982; ZENK, 1975; ZENK and ARMI, 1990; RHEIN and HINRICHSEN, 1993).

Despite having the densest source water of the four major outflows considered here, the Mediterranean outflow does not sink to the bottom of the North Atlantic because it entrains a substantial volume of the overlying North Atlantic Central Water (NACW) while still in the Gulf of Cadiz (SMITH, 1975). This entrainment reduces its salinity and density so that the product water that finally reaches the open North Atlantic has a density $\sigma_{\theta prd} = 27.6 \pm 0.1 kg\ m^{-3}$ making it neutrally buoyant at depths from about 800 to 1300m in the main thermocline (HEEZEN and JOHNSON, 1969). Even so, the Mediterranean outflow water is still considerably saltier and warmer than other thermocline water types (Labrador Sea Water and Antarctic Intermediate Water) and forms a conspicuous anomaly that can be traced northwards along the eastern boundary of the northern North Atlantic, and southwestwards across the subtropical North Atlantic (WORTHINGTON 1975; REID, 1979).

3.1 Simulation results

To simulate the descent of the Mediterranean outflow into the North Atlantic the model outflow is initialized with the properties observed at the west end of the Strait of Gibraltar (PRICE *et al*, 1993) (35.9°N, 6.25°W), $\theta = 13.4°C$, S = 37.8, $U = 1.0 m\ s^{-1}$ to the west-southwest, and H = 100m. The width is chosen to give the observed transport, roughly $1.0 \times 10^6 m^3 s^{-1}$, and hence W = 10km which is consistent with a visual estimate of width. The transport of salinity anomaly (above 36.1) is thus 1.7Sv%, in the units of BRYDEN *et al* (1994), and fairly close to their long-term mean. The oceanic profiles of temperature and salinity are taken from CTD observations of KENNELLY, SANFORD and LEHMAN (1989) (the shallower portion from 0-400m is profile 84 from the eastern Gulf of Cadiz, and the deeper portion to 1500m is profile 135 from the western Gulf of Cadiz). Once initialized, the simulated outflow is allowed to flow into the Gulf of Cadiz along a path that is determined by the model dynamics and by the bottom topography (Fig.4). The outflow temperature, salinity and speed change considerably as the outflow descends the continental slope (Figs 5,6 and 7). To understand why these changes occur it is helpful to imagine following a single column.

The starting location is on the continental shelf where the bottom slope is fairly gentle, $\alpha \approx 4 \times 10^{-3}$. The current is flowing southwestward in a narrow channel that confines its width to be something less than would be given by the broadening parameterization (Eq.8). To account for this, the broadening parameter, β, is set to 0.2 for the first 20km of the path. The channel ends at the edge of the continental slope, where the outflow moves onto more or less open topography and β reverts to the nominal form, $\beta = 2K$.

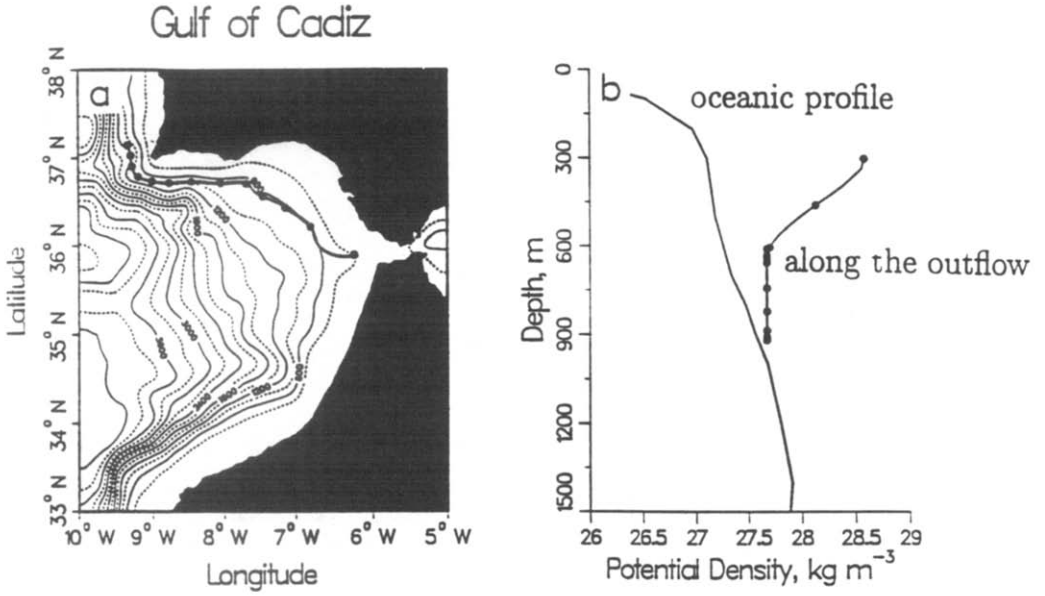

FIG.4. (a) The path of the simulated Mediterranean outflow. The outflow begins at the western end of the Strait of Gibraltar and flows westward through the Gulf of Cadiz. Dots along the track are at intervals of half a day. The path of the simulated outflow is insensitive to variations of the initial condition. (b) Potential density profiles in the oceanic water column (Gulf of Cadiz) and along the path of the simulated outflow. In the latter case the density is plotted as a function of the bottom depth and the dots along the curve are at 25km intervals. Note that the outflow density intersects the oceanic density at a depth of about 1000m, at which point the outflow is neutrally buoyant.

The Froude number of the initial condition is just below 1, and there is no entrainment at the start (though the initial properties indicate that the outflow has already begun to mix with NACW, probably at the main sill (ARMI and FARMER 1988)). As the current flows onto the continental slope the topographic acceleration increases substantially as the bottom slope increases to about $\alpha_{max} = 12 \times 10^{-3}$. In response, the current speeds up slightly, reaching a maximum of about 1.2m s^{-1}, and the outflow also begins to broaden (Fig.7c), which reduces the column height. The combined effect of the acceleration and broadening is to raise the Froude number above 1, which, together with the larger bottom slope, causes fairly intense entrainment of overlying NACW. In total, the outflow entrains about $1.8 \times 10^6 m^3 s^{-1}$ of NACW from the temperature range 11.4 to 12.5°C, and salinity range 35.6 to 35.7. This entrainment of NACW causes a slight cooling of the outflow to 12.45°C and a marked salinity decrease to 36.45 within about 50km of the starting location (Fig.6b). This reduction of salinity, combined with the descent of the outflow, reduces the density difference between the outflow and the overlying NACW from its initial value of about 1.5kg m^{-3} to about 0.5kg m^{-3} at around 50km downstream of the start (Figs 4b and 5b).

All of this entrainment happens within half a day of the outflow exiting the Strait of Gibraltar, as it descends from the sill depth of about 350m to a bottom depth of about 600m. The observations of HEEZEN and JOHNSON (1969), SMITH (1975) (plotted in Fig.5b) and PRICE *et al* (1993) show a similar rapid decrease of salinity and density in this region. In our simulation this strong entrainment is a direct consequence of the stronger topographic acceleration of the continental slope, and is enhanced by the effect of broadening.

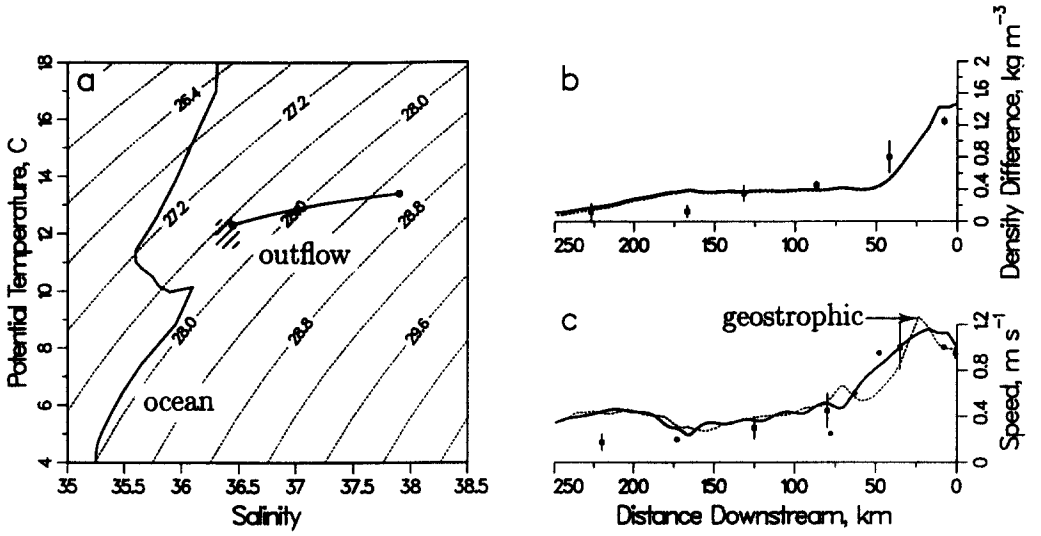

FIG.5. (a) Θ-S diagram for the oceanic profile (Gulf of Cadiz) and along the path of the simulated outflow. The initial values for the outflow are 13.4°C and 37.8, and the product water values are within the shaded region which shows the approximate range of Θ-S observed in the Mediterranean outflow near Cape St Vincent. (b) Density difference (outflow minus oceanic) along the path of the simulated outflow. The solid curve is the potential density difference, which may be compared with SMITH's (1975) analysis of MADELAIN's (1970) sections I through VI (the six data points from right to left). The dashed curve (which is almost indistinguishable in this case) is the *in situ* density difference used to compute the buoyancy of the outflow within the numerical model. In this and in all subsequent along-stream profiles the origin is placed at the right side of the diagrams. (c) Speed along the path of the outflow. The solid curve is the simulated current speed; the dashed curve is the geostrophic speed, $g'\alpha/f$. The simulated and the geostrophic speeds differ by about 25% near the start, but become nearly equal within about 75km downstream. The simulated current may be compared with observed speeds taken from the compilations of SMITH (1975) (the points with error bars) and HEEZEN and JOHNSON (1969) (those without). The speed within the real outflow is undoubtedly sensitive to the depth and location of the measurement, which is not accounted for in this comparison and which should therefore be interpreted as semi-quantitative.

Entrainment ceases entirely in the simulation once the Froude number drops below 1 (Fig.7c) at about 50km downstream of the start where the current decelerates to about 0.4m s^{-1} (Fig.5c). The deceleration results from both the loss of density difference noted above, and a northward (rightward) change of direction caused by the Coriolis acceleration which banks the current up against the continental slope along the northern flank of the Gulf of Cadiz. Thereafter, the outflow continues to flow along the northern side of the Gulf of Cadiz as a nearly geostrophic current. It is slightly damped by bottom friction ($K \approx 0.2$) and slowly crosses isobaths until it becomes neutrally buoyant at a depth of about 1000m in the vicinity of Cape St Vincent (Fig.4b). The simulated product water properties are $\Theta_{prd} = 12.45°C$, $S_{prd} = 36.45$, $\sigma_{\theta prd} = 27.64 kg\ m^{-3}$, and $M_{prd} = 2.8 \times 10^6 m^3 s^{-1}$, which are within the fairly broad range of observed values (ZENK and ARMI, 1990; OCHOA and BRAY, 1991). In this case, the model seems to have the essential dynamics required to simulate both the product water properties, and the highly localized character of mixing along the outflow path.

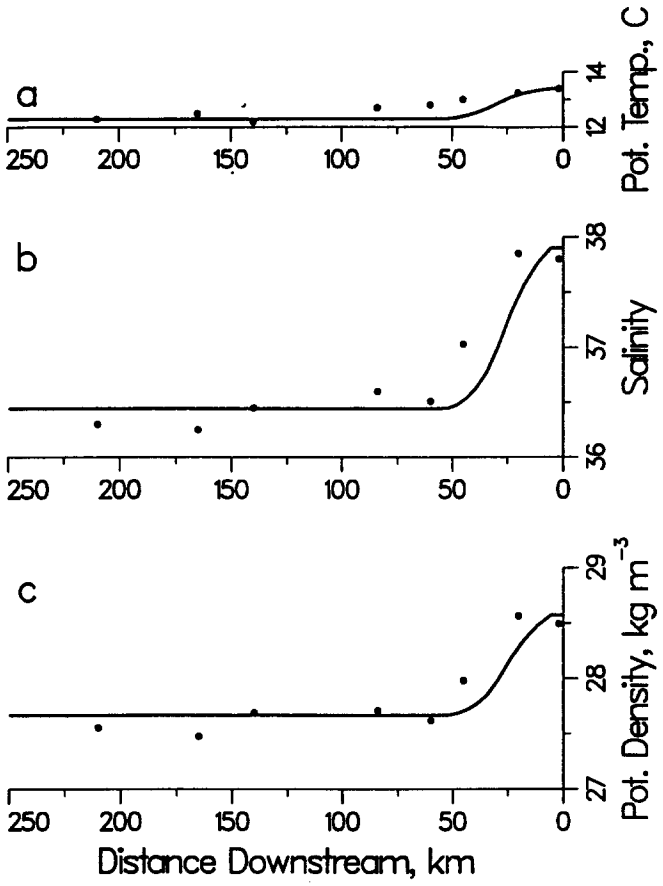

FIG.6. (a) Temperature along the path of the Mediterranean outflow. The solid curve is from the simulation and the data points are the velocity-weighted estimates from field data described by PRICE *et al* (1993) and BARINGER (1993). (b) Salinity as in (a). (c) Potential density. The scales in (a) and (b) are proportional to their contribution to potential density. Note the rapid decrease of outflow potential density in the interval from about 20 to 50km downstream. The same rapid decrease is evident in the potential density difference of Fig.5b, which also shows a continued steady decrease further downstream because of the outflow's descent into a stratified oceanic water column.

The simple end-point model of an entraining density current also gives a fairly consistent account of the source to product water conversion in the Mediterranean outflow. Noting that the maximum bottom slope is $\alpha_{max} = 12 \times 10^{-3}$, and other parameters listed in Table 1, then $\Phi = 0.58$. Thus the volume transport of product water would be expected to be about $1/(1-\Phi) = 2.4$ times the initial (or source water) transport, and the product water would be a mixture of about 40% source water, and 60% oceanic water, which are close to the results found in the numerical simulation (Fig.7d).

3.2 Numerical experiments; sensitivity to source Θ-S

Having simulated the outflow using modern source conditions, we now briefly consider some numerical experiments in which one or more of the external variables are changed to values which may have occurred in the geological past. For example, in the introduction we noted the occurrence of saline (rather than cold) North Atlantic bottom waters about 50 million years ago. This poses

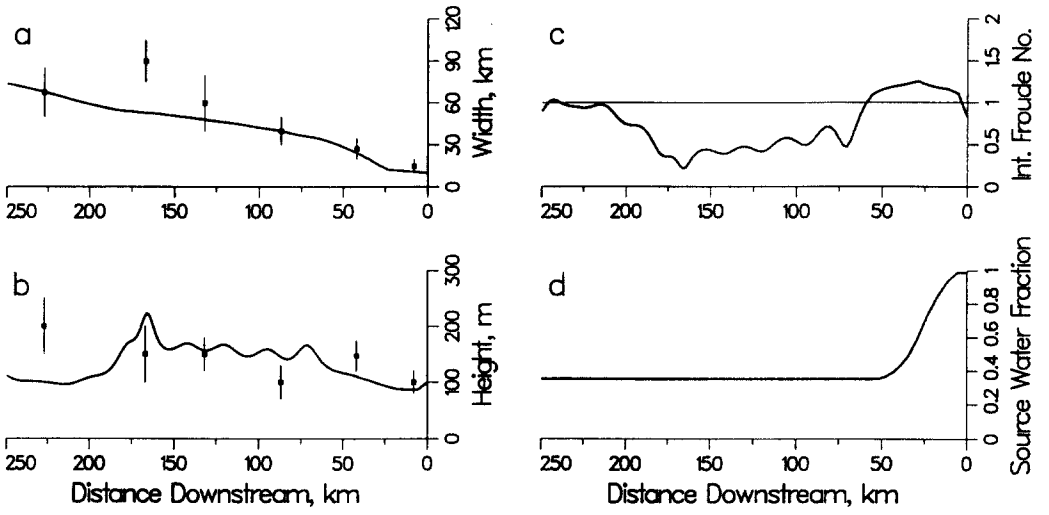

FIG.7. Some bulk properties of the Mediterranean outflow. (a) Width (solid line) and an estimate of the observed width made from MADELAIN's (1970) Fig.1 at sections I through VI (data points from right to left). (b) Column height (solid line) and an estimate of observed height made from MADELAIN's (1970) sections. The Mediterranean outflow was identified by salinities in excess of 36.4. (c) Internal Froude number. (d) Source water fraction. The simulated height and width increase downstream so that the cross-sectional area of the outflow increases by about a factor of about seven. This increased area combined with the decreased speed (Fig.5c) gives a constant downstream flux of source water.

the question - What source salinity would be required to produce bottom waters from the present Mediterranean outflow? Or a little more generally - How does the (simulated) Mediterranean product water change in response to variations of the Mediterranean source water? To examine this we simply change the initial Θ-S and rerun the simulation holding other initial conditions fixed at their nominal values.

If the change in Θ-S leaves the density unchanged, then the dynamics are unchanged and the product water properties can be computed from a relation like Eq.22-24 with Φ unchanged. However, if the source water density is changed, say by increasing the source salinity by 1 to S_{src} = 38.9, then the product salinity and density are found to increase, as expected. However, the increase of the product salinity and density are very small; in the case mentioned S_{prd} = 36.5, and $\sigma_{\theta prd}$ = 27.76kg m^{-3} so that $\partial\rho_{prd}/\partial\rho_{src}$ = 0.12 and 88% of the imposed density anomaly is lost in the product density[1]. This remarkable insensitivity to variations of the source density could have been anticipated from the solution of the end-point model, Eq.27, by noting that $\partial\rho_{prd}/\partial\rho_{src}$ = (1-Φ)/3 = 0.15, or about the same as found in the numerical experiments (and recall the discussion in Section 2.2.3 following Eq.27).

[1]This shows that if the nominal simulation had been initialized with pure Mediterranean water, Θ = 13.5°C and S = 38.45, then the product water would have been almost indistinguishable from the result noted above where the source water was slightly mixed Mediterranean water. In cases where the source density is made larger, the simulated outflow shows a second region of entrainment at about 250-300km downstream where the continental slope is very steep. HEEZEN and JOHNSON's (1969) classic Fig.30 indicates a second region of minor salinity decrease in that region. Whether this secondary entrainment event is treated realistically by the one-dimensional model is questionable, since by then the outflow has broadened considerably, and some of the real outflow has already begun to float off the bottom.

TABLE 1: Parameters and results of the End-Point Model

	Mediterranean	Denmark Strait	Faroe Bank Channel	Filchner Ice Shelf
Source properties:				
H, m	100	150	150	100
U, m s^{-1}	1.0	0.35	0.8	0.1
W, km	10	50	15	100
Θ, °C	13.4	0.0	-0.5	-2.1
S	37.80	34.90	34.92	34.67
σ_θ, kg m^{-3}	28.48	28.03	28.07	27.92
σ_1, kg m^{-3}	32.91	32.77	32.83	32.73
B, $m^3 s^{-3}$	1.35	0.19	0.83	0.01
Oceanic conditions:				
Θ, °C	12	3.7	7	0.5
S	35.60	34.90	35.15	34.68
σ_θ, kg m^{-3}	27.06	27.72	27.56	27.82
σ_1, kg m^{-3}	31.25	32.39	32.11	32.56
Site parameters:				
f, 10^{-5} s^{-1}	8.4	13.3	12.9	13.9
X_e, km	30	100	250	100
α_{max}, 10^{-3}	12	28	15	32
Z_e, m	300	750	850	1000
$\delta\sigma_{Ze}$, kg m^{-3}	1.41	0.38	0.65	0.18
Flow parameters:				
U_{geo}, m s^{-1}	2.1	0.80	0.92	0.39
B_{geo}, $m^3 s^{-3}$	0.67	0.12	0.12	0.009
K_{geo}	0.2[a]	0.2	0.2	0.1
F_{geo}	3.7	2.0	2.1	2.6
Φ	0.58	0.36	0.46	0.46
Product water properties:				
Θ, °C	12.6	1.5	3.0	-0.9
S	36.52	34.91	35.00	34.67
σ_θ, kg m^{-3}	27.67	27.96	27.91	27.90
σ_1, kg m^{-3}	32.10	32.65	32.55	32.66
σ_4, kg m^{-3}	44.81	46.04	45.95	46.24

[a]This is an effective K that represents the channel constraint upon broadening described in Section 3.1. The geostrophic K is much larger than this at the start, $K_{geo} \approx 1.1$, which would indicate more broadening than can actually occur.

An imposed density anomaly has a bigger effect on the volume of transport of the product water. In the experiment above, where $S_{src} = 38.9$, the source density is increased by about 0.7kg m^{-3}, and the product water transport increases to $M_{prd} = 3.7 \times 10^6 m^3 s^{-1}$, considerably larger than in the nominal result. Numerical experiments give that $\delta\rho/M_{src}(\partial M_{prd}/\partial\rho_{src}) = 1.5$ while the derivative of the solution of the end-point model yields $\delta\rho/M_{src}(\partial M_{prd}/\partial\rho_{src}) = 2/3(1-\Phi)^{-1} = 1.6$. This comparatively large increase in the volume transport of product water is a direct consequence of the increase in entrainment.

To return to the question of saline bottom water, the answer suggested by these simulations is that even $S_{src} = 42$ is not sufficient to produce bottom water under present conditions. Still further increases of the source salinity result in very little increase in product water density since by then $\Phi \approx 1$. The relatively warm temperature of the Mediterranean product water also acts to keep this outflow from sinking to the bottom because the *in situ* density difference decreases as the ambient pressure increases (REID and LYNN, 1971; KILLWORTH, 1977; and more on this in Section 5.2). Thus, on the basis of this model, the occurrence of highly saline North Atlantic bottom water in the past can not be attributed solely to an increase of Mediterranean salinity. Many other factors may have played a significant role including the oceanic density profile, sea level relative to sill depth and thermocline depth, and the temperature difference between Mediterranean product water and other deep water types.

4. THE NORWEGIAN-GREENLAND SEA OUTFLOWS

The deep and bottom waters of the northern North Atlantic have their source in outflows from the Norwegian-Greenland Sea (LEE and ELLETT, 1965, 1967; SWIFT, AAGAARD and MALMBERG, 1980; SWIFT, 1984a). Winter cooling combined with inflows from the Arctic makes several types of very dense source water, the densest of which is Norwegian Sea Deep Water (AAGAARD, SWIFT and CARMACK, 1985). A slightly less dense source water - Arctic Intermediate Water, is produced by air-sea interaction in the central Greenland basin (SWIFT and AAGAARD, 1981). These two water types fill the basins up to the level of the Scotland-Iceland-Greenland Ridge, and overflow southward into the North Atlantic (PETERSON and ROOTH, 1976; LIVINGSTON, SWIFT and OSTLUND, 1985; LIVINGSTON, 1988). The Arctic Intermediate Water outflows primarily through Denmark Strait, which has a sill depth of about 600m. The slightly denser Norwegian Sea Deep Water outflows mainly through the Faroe Bank Channel south of the Faroe Islands where the sill depth is about 800m (CREASE, 1965; SAUNDERS, 1990; BORENÄS and LUNDBERG, 1988), and intermittently over the Iceland-Faroe Ridge which has a depth of about 500m (MALMBERG, 1985; WILLEBRAND and MEINCKE, 1980).

4.1 Denmark Strait Outflow

The hydrography and the dynamics near the source of the Denmark Strait outflow appear to be very complex by comparison to the other outflows, and even the composition of the source waters is not completely clear-cut. Both the East Greenland Current and the Arctic Intermediate Water flow southward through Denmark Strait (i.e. there is not a simple two-layer exchange flow) so that there is no obvious boundary defining the source water; also the currents within the Strait are highly variable over periods of a few days to a week (WORTHINGTON, 1969; ROSS, 1984). Nevertheless, based upon the time-averages observed by ROSS (1984) the Denmark Strait source water is estimated to have an average Θ-S west of Iceland (very near Section II of the 1967 Hudson expedition, hereinafter H67, GRANT, 1968) that are about 0°C and 34.90. The average amplitude

of the current is about 0.35m s^{-1} towards the southwest, the height is about 150m and the average volume transport near the sill is about 2.6 x $10^6 m^3 s^{-1}$ which gives a width of 50km. The effects of transport variations are discussed below.

Once the outflow reaches deeper water in the Irminger Sea it forms a distinct, cold bottom layer having a substantial southward geostrophic flow along the continental slope of Greenland (SMITH, 1975; DICKSON, GMITROWICZ and WATSON, 1990). This outflow retains a significant density difference with respect to the overlying water as it descends all the way to the deep ocean floor in the northwestern North Atlantic. MANN (1969) analyzed the H67 hydrographic data to define the Θ-S properties of the outflow water near Cape Farewell, where most of the outflow has settled to the bottom of the Labrador Basin. The mid-range Θ-S was found to be 1.5°C and 34.91, which define Northwest Atlantic Deep Water (NWADW), but there is a fairly large range of Θ-S variation across the instantaneous outflow. Mann found that temporal variation over a period of several years around 1968 was small by comparison, though variations have been observed over longer periods (BREWER, BROECKER, JENKINS, RHINES, ROOTH, SWIFT, TAKAHASHI and WILLIAMS, 1983; SWIFT, 1984b).

4.1.1. Denmark Strait Simulation Results. The simulated outflow is started very near the location of H67 Section II (Figs 8 and 9) with the source water properties noted above. The oceanic profile is H67 station 109 (MANN, 1969, Fig.8).

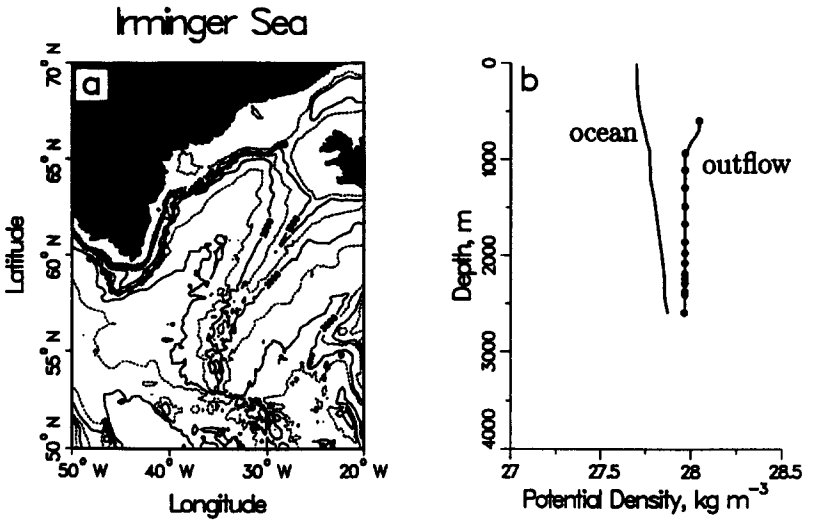

FIG.8. (a) Simulated path of the Denmark Strait outflow. The outflow is initialized to the west of Iceland and flows southward along the continental slope of Greenland. Dots along the track are at intervals of three days. As in the previous case, variations of the initial condition cause no perceptible change in the simulated path. (b) Potential density profile in the oceanic water and along the path of the outflow. In the latter case the density is plotted as a function of the bottom depth and dots are at intervals of 100km. Note that the outflow density does not intersect the oceanic density profile and this outflow continues to the sea floor in the northern North Atlantic.

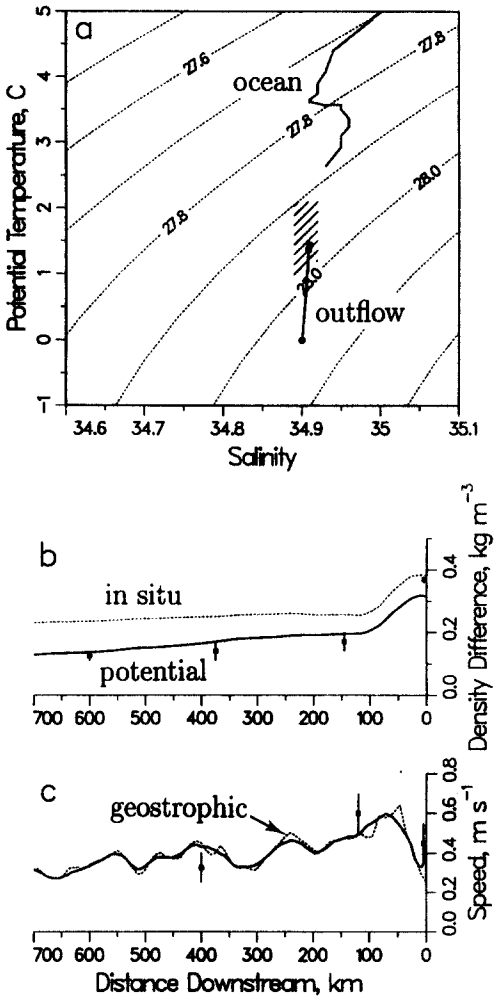

FIG.9. (a) Θ-S diagram for the oceanic profile (Irminger Sea) and along the path of the simulated Denmark Strait outflow. The starting value for the outflow is 0°C and 34.90, and the product water values are within the shaded region which shows the approximate range of Θ-S observed within the Denmark Strait outflow near Cape Farewell by MANN (1969). (b) Density difference (outflow minus oceanic) along the path of the simulated outflow. The solid curve is the potential density difference, which may be compared with SMITH's (1975) analysis of the Hudson 1967 data (the data points are from Sections II through V, from right to left). The dashed curve is the *in situ* density difference used to compute the buoyancy of the outflow within the model. Note that the *in situ* density difference is somewhat larger than the potential density difference because the outflow water is colder than the oceanic water and thus has a greater compressibility at depth (or a smaller expansion coefficient). (c) Speed along the path of the outflow. The solid curve is the simulated current speed; the dashed curve is the geostrophic speed, $g'\alpha/f$, which is nearly equal in this case. The simulated current may be compared with observed speeds taken from current meter array data by ROSS (1977, 1984) (the data points at about 0 and 130km downstream) and from DICKSON *et al* (1990) (the point at about 400km downstream). As in the previous case, comparisons of speeds are semi-quantitative.

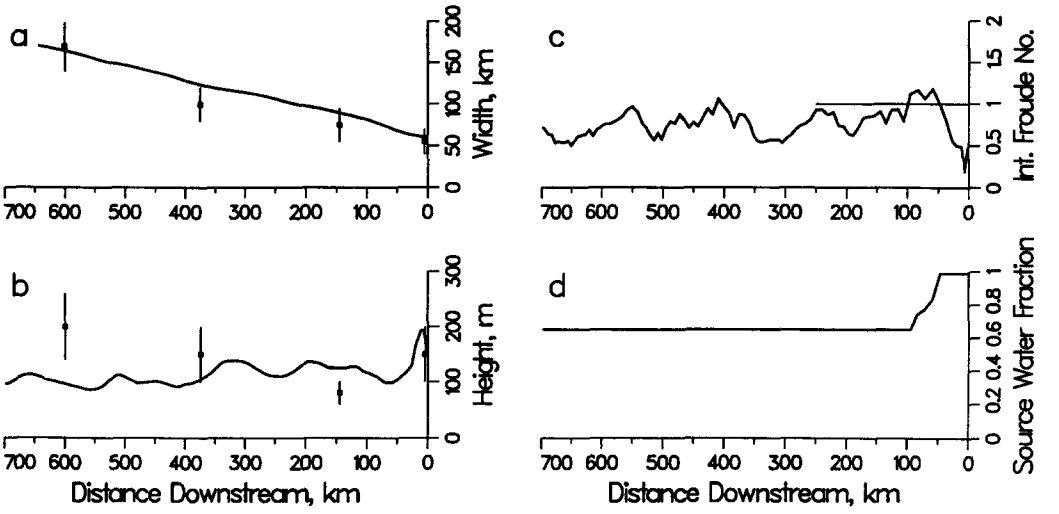

FIG.10. Some bulk properties of the Denmark Strait outflow. (a) Simulated width (solid line), and an estimate of the observed width made from MANN's (1969) Figs 2,3,4 for sections II through V (the four data points from right to left). The Denmark Strait outflow water was identified with bottom salinities less than 34.94. (b) Column height and an estimate of observed column height as in the previous plot. The height and width increase downstream so that the cross-sectional area of the outflow increases by about a factor of about three when the outflow reaches Cape Farewell. The cross-section of the outflow seen in SMITH's (1975) analysis increases somewhat more than this, but may include a contribution from the Iceland-Scotland outflow. (c) Internal Froude number. (d) Source water fraction.

The Froude number of the initial outflow is well below 1 (Fig.10), and the outflow is nonentraining until it encounters steep topography just beyond the shelf-slope break about 50km downstream where $\alpha_{max} \approx 28 \times 10^{-3}$. This causes the current to accelerate to a maximum speed of about 0.6m s^{-1}. This higher speed, combined with broadening of the flow, raises the Froude number above 1 and causes substantial entrainment. The volume transport increases to about $4.1 \times 10^6 m^3 s^{-1}$ through entrainment of oceanic water having properties $\Theta = 3.5$ to 4.0°C, $S \approx 34.92$, and $\sigma_\theta \approx 27.75 kg\ m^{-3}$, i.e. Irminger Sea Water (LEE and ELLETT, 1965) which might also be characterized as a slightly salty version of Labrador Sea Water. This entrainment of warmer and slightly saltier water warms the outflow to about 1.49°C and increases its salinity almost neglibly to 34.91. All entrainment is completed within about 100km of the start, and the simulated outflow shows no further changes in Θ or S as it flows southward along the continental slope of Greenland. The simulated product water Θ-S properties are nearly in the middle of the observed range reported by MANN (1969).

Within the simulation, entrainment occurs over a localized portion of the outflow path between H67 Sections II and III and is sufficient to reduce the potential density of the outflow by about 0.1kg m^{-3}. SMITH (1985) analyzed the H67 data to estimate the potential density difference of the outflow with respect to the surrounding oceanic water, and his estimates for Sections II through V are shown in Fig.9b (the same sort of data were shown in Fig.5b). These data show a relatively rapid decrease of the density difference in this region, though recall that the density difference can decrease because of both entrainment and descent of the outflow into a stratified, oceanic environment (Fig.8b, Eq.5). In any case, the H67 data are too sparsely distributed for the purpose of deducing where entrainment may occur. However, the observations are consistent with there being very little entrainment downstream of Section III, since the very slow decrease of the potential density difference observed south of Section III is simulated well by the model where it results from descent alone (and assuming that the model's oceanic density profile is correct).

The momentum balance is nearly geostrophic all along the path (Fig.9c), though bottom friction is crucially important in allowing the overflow to descend the continental slope. By the time the simulated outflow has reached the southern tip of Greenland it has descended to the continental rise at about 2700m depth and still retains a significant density difference with respect to the surrounding oceanic water.

4.1.2. Numerical experiments; sensitivity to initial transport. ROSS (1984) observed that the thickness and current of the outflow west of Iceland varied by a factor of two or more on a several day to weekly period. Since the outflow requires only about two days to reach the entrainment region (just beyond the shelf-slope break), these very large variations of initial speed and thickness might be expected to alter the magnitude of entrainment and thereby the product Θ-S.

Numerical experiments show that if either the initial speed or layer thickness are increased, the entrainment is somewhat less, so that the product water remains cooler. The sensitivity can be measured by $\partial\Theta_{prd}/\partial H_{src} = 5.9 \times 10^{-3}$C m^{-1} and $\partial\Theta_{prd}/\partial U_{src} = 1.4 \times 10^{-2}$C m^{-1} s, or in a nondimensional form, $\partial \ln(\Delta\Theta)/\partial \ln U_{src} = 0.48$, and $\partial \ln(\Delta\Theta)/\partial \ln H_{src} = -0.53$, where $\Delta\Theta = \Theta_{prd} - \Theta_{src}$ is the change in outflow temperature resulting from entrainment. The nearly similar magnitude and sign of the nondimensional forms suggest that the important effect of varying U_{src} or H_{src} is to vary the initial transport per unit width, Q_{src}. This can be checked by numerical experiments, and indeed covariations of U_{src} and H_{src} that keep the transport constant have little effect on the properties of the product water. This equivalence of U_{src} and H_{src} is perhaps surprising, but can be understood as a consequence of the nearly geostrophic momentum balance that characterizes the simulated outflows. Because the momentum balance is nearly geostrophic (rather than inertial), the current speed at the entrainment site is determined mainly by the density difference of the outflow (and α and f, of course), and not by the initial speed of the outflow. The initial speed is still of some importance since together with H it determines the transport, Q, and that in turn determines the column height by continuity (Eq.6 or the equivalent for the end-point model, Eq.14). In this important respect, outflows are better thought of as density-driven plumes rather than as inertial jets which their high initial speeds might lead one to infer.

For the present purpose it is sufficient to consider only variations of the initial transport, and experiments indicate that the nondimensional sensitivity is $\partial \ln \rho_{prd}/\partial \ln Q_{src} \approx -0.5$, which is probably significant given the O(1) changes observed in the initial transport (ROSS, 1984). That is, from the numerical experiments, we expect that the product water temperature would vary significantly, by O(1/2°C), if the initial transport variations are O(1) as they appear to be. There are reports of relatively undilute blobs of source water being found along the path of the outflow (COOPER, 1955; SWIFT, 1984a) which might result from intermittent enhanced transport through the Strait. Nevertheless, on balance this model result appears to be at odds with MANN's (1969)

finding of minimal temporal variation of outflow properties near Cape Farewell (minimal, that is, compared to the very large transport variations near the sill). It may be that short-term variations of Θ-S are smeared out before the outflow reaches Cape Farewell (roughly 30 days downstream from the start), perhaps by shear-enhanced dispersion, which is not treated in this one-dimensional model.

4.2 Faroe Bank Channel outflow

The Faroe Bank Channel outflow is the lower layer of a two-layer exchange flow between the North Atlantic and the Norwegian Sea (CREASE, 1965; BORENÄS and LUNDBERG, 1988; SAUNDERS, 1990). The source water properties are fairly well defined, Θ = -0.5°C, and S = 34.92, and very close to that of Norwegian Sea Deep Water. The outflow current is west-northwestward through the narrow Faroe Bank Channel at a rate of about 0.8m s^{-1}. The outflow has a height of about 150m and a volume transport of about 1.7 x $10^6 m^3 s^{-1}$ (BORENÄS and LUNDBERG, 1988; SAUNDERS, 1990) indicating a width just at the west end of the channel of about 15km. The outflow moves westward along the Iceland-Faroe Ridge, and by the time it reaches the Reykjanes Ridge has been modified to Northeast Atlantic Deep Water (NEADW) which has central Θ = 2.6°C and S = 35.0. This product water is markedly warmer and saltier than the NWADW from Denmark Strait.

4.2.1. Faroe Bank Channel simulation results. Oceanic temperature and salinity are specified by GEOSECS profile 23 from the central Icelandic Basin. The deepest several hundred meters (depths from about 2300m to 2500m) of this 'oceanic profile' are NEADW which covers the sea floor throughout most of the basin. The simulated outflow does not descend below about 1500m while within the model domain (Fig.11) and hence is not influenced by the bottom water properties of the oceanic profile. The simulated outflow is started just to the west of the narrow Faroe Bank Channel on topography that slopes up to the north as part of the Iceland-Faroe Ridge. The outflow adjusts quickly to a damped geostrophic balance and flows westward along the ridge, descending only slightly. Though the initial Froude number is close to 1, the gentle slope of the Iceland-Faroe Ridge does not cause any further acceleration of the current, and the simulated outflow does not undergo significant entrainment until it flows over steep topography just east of Iceland ($\alpha_{max} \approx$ 15 x 10^{-3}), about 300km from the start. There the current accelerates to speeds of about 0.6ms^{-1}, increasing the Froude number to 1, and the outflow entrains about 1.9 x $10^6 m^3 s^{-1}$ of overlying North Atlantic water which is much warmer and saltier, having Θ ≈ 7°C and S ≈ 35.2, i.e. Upper North Atlantic Deep Water (WÜST, 1935). This entrainment warms the outflow to about 2.8°C and increases its salinity to about 34.98 (Fig.12). No further entrainment occurs as the outflow continues southward along the eastern flank of the Reykjanes Ridge so that it retains a substantial density difference.

The product water Θ-S found in the simulation are roughly consistent with those of NEADW (Fig.12). However, the simulation appears to be in error by having the site of the entrainment farther downstream than observations suggest. Historical data presented by HARVEY and THEODOROU (1986) indicate that the change of Θ-S properties within this outflow occurs rather gradually as the outflow moves westward along the Iceland-Faroe Ridge. We are not sure why the actual and the simulated outflows differ in this regard, but suspect that the simplified dynamics of the momentum balance or the broadening parameterization are likely to be at fault. This outflow becomes considerably thinner as it first spreads out after exiting the Faroe Bank Channel. The resulting along-stream baroclinic pressure gradient would tend to accelerate the current in a way that is ignored by this simple model, and the time-dependent (inertial) broadening that may occur is also omitted.

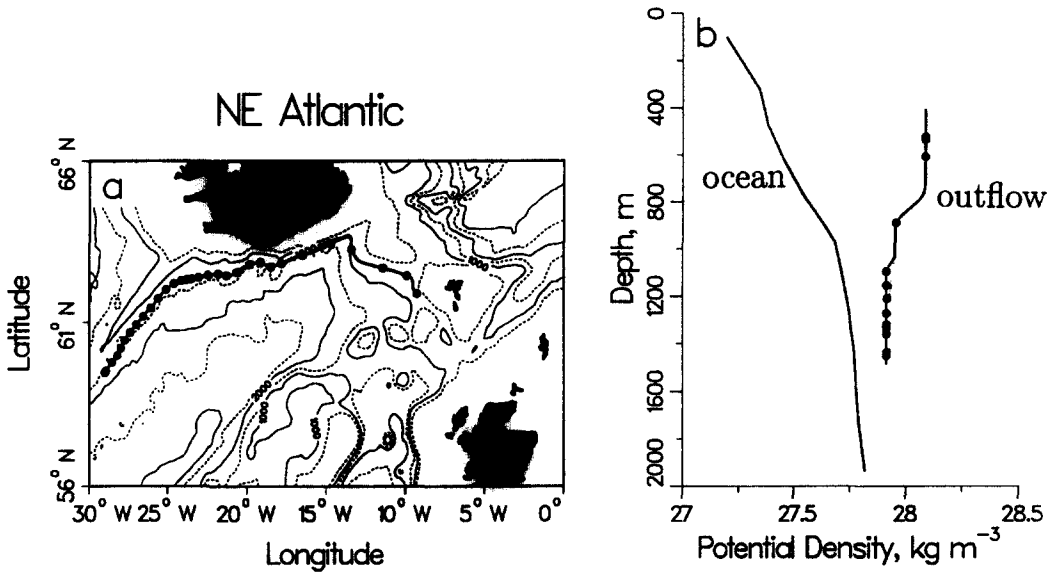

FIG.11. (a) Simulated path of the Faroe Bank Channel outflow. The outflow is started just west of the Faroe Islands and flows northwestward along the Iceland-Scotland Ridge and southwestward along the Reykjanes Ridge. Dots are at three day intervals. (b) Density profiles as in Fig.8b. The simulated outflow is still descending as it flows southwestward along the Reykjanes Ridge and does not reach neutral buoyancy or the sea floor while within the model domain.

As well, there may be other mixing processes which are not directly related to outflow dynamics, e.g. tidally-driven bottom mixing. To sort out which of the many possibilities actually obtain it would be most valuable to directly measure the currents and the turbulence intensity within this outflow.

While the numerical model seems to be in error at simulating the site of the entrainment, the solution of the end-point model, Eq.26, suggests that this may not invalidate the simulation of the product water properties. That is, even if the outflow begins to entrain before reaching the steep topography of the Reykjanes Ridge, it would nevertheless be expected to have the same product water properties after traversing that topography.

In the same way, the intermittent overflow of about $1 \times 10^6 m^3 s^{-1}$ of source water across the Iceland-Faroe Ridge (MEINCKE, 1983) would be expected to join the path of the Faroe Bank Channel outflow and undergo the same entrainment and modification. This ridge overflow would result in product water indistinguishable from that coming from Faroe Bank Channel, assuming that its source properties were roughly the same. The combined southward flow of product water along the eastern flank of the Reykjanes Ridge, which is called the Iceland-Scotland outflow, would then have a transport of about $1.7 + 1.9 + 1.0\,(1 + 1.9/1.7) = 5.7 \times 10^6 m^3 s^{-1}$, which is roughly consistent with the transport observed by STEELE, BARRINGTON and WORTHINGTON (1962).

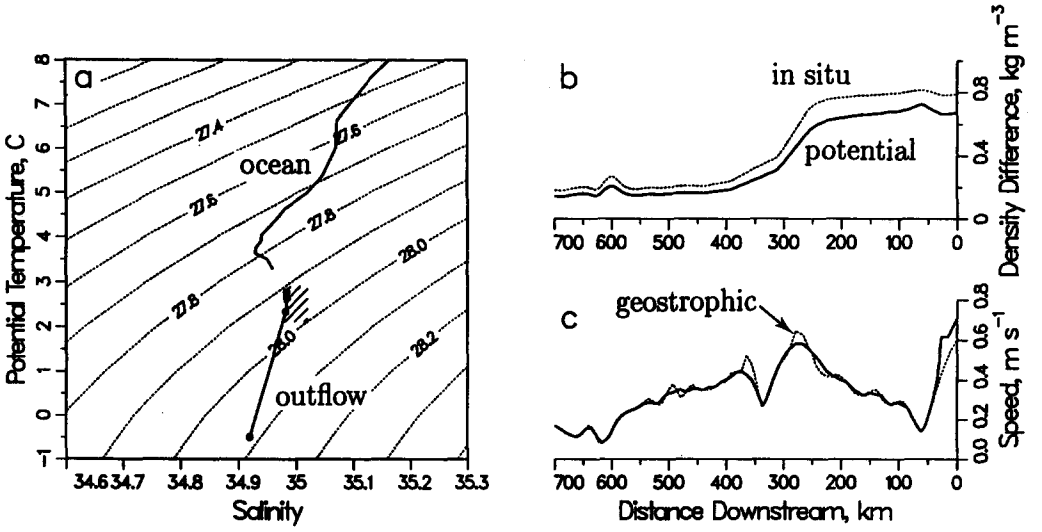

FIG. 12. (a) Θ-S diagram for the oceanic profile (central Icelandic Basin) and along the path of the simulated Faroe Bank Channel outflow. The simulated outflow is started with Θ = -0.5°C, and S = 34.92 and the product water values are barely within the shaded region which shows the approximate range of Θ-S observed in the Iceland-Scotland outflow. The deepest several hundred meters of the oceanic profile have been omitted here for clarity. (b) Density difference (outflow minus oceanic) along the path of the simulated outflow. The solid curve is the potential density difference, and the dashed curve is the *in situ* density difference. We believe that the model solution is in error in that it shows entrainment occurring mainly where the outflow encounters the Reykjanes Ridge about 250km from the starting point. Observations suggest that significant entrainment occurs along the Iceland-Scotland Ridge. (c) Simulated speed along the path of the outflow (solid curve) and the geostrophic speed (dashed curve).

4.2.2. Numerical experiments; sensitivity to oceanic conditions. Though the Faroe Bank Channel and Denmark Strait outflows begin with nearly equal temperature, salinity and density, the resulting product waters are distinct as noted in the introduction. The main reason, pointed out by LEE and ELLETT (1967) is that these outflows descend through quite different oceanic environments. The subsurface waters to the west of the Reykjanes Ridge (south of Denmark Strait) are mainly of subpolar origin (Labrador Sea Water), and at depths of about 800 to 1000m, where the majority of entrainment occurs in either case, have temperature and salinity of roughly 3.5 to 4.0°C and 34.9. To the east of the Reykjanes Ridge the oceanic water at the same depths is of North Atlantic origin and is much warmer and saltier, typically about 7°C and 35.2. If the oceanic profiles in the two simulations are arbitrarily switched, then the simulated Denmark Strait outflow produces something like NEADW (Θ = 3.3°C and S = 34.99), while the Faroe Bank Channel outflow produces a rather warm version of NWADW (Θ = 2.3°C and S = 34.92). This indicates the crucial role of the oceanic properties in determining the product water of a marginal sea outflow.

4.3 North Atlantic Deep Water

The Iceland-Scotland outflow continues southward along the Reykjanes Ridge until reaching the Gibbs Fracture Zone where it flows westward into the Irminger Sea at a depth of about 2000m. The Iceland-Scotland outflow joins the Denmark Strait outflow to make up the deep core of the Deep Western Boundary Current that continues southward along the continental slope of North America (SMETHIE, 1993). Given the volume transports of source and oceanic water noted above, the volume transport of the combined deep water flow is estimated to be $9.7 \times 10^6 m^3 s^{-1}$ having a mean temperature of 2.4°C, and a mean salinity of 34.95. This estimated transport is slightly less than the measured transport of water having $\sigma_\theta \geq 27.8$, $10.7 \times 10^6 m^3 s^{-1}$, found by DICKSON *et al* (1990) at a site about 400km south of H67 Section II. (It should be kept in mind that the model simulates only the additional transport added by entrainment, and the depth (or density) range of the water entrained.) The combined flow of 'new' lower NADW (the full NADW includes a contribution from the Labrador Sea as well, TALLEY and MCCARTNEY (1982)) thus has a composition:

27% Denmark Strait source water (mainly Arctic Intermediate Water),

17% oceanic water entrained by the Denmark Strait outflow (Irminger Sea Water),

26% Iceland-Scotland source water (mainly Norwegian Sea Deep Water),

30% oceanic water entrained by the Iceland-Scotland outflow (Upper North Atlantic Deep Water).

Sometime during the 1970s the Θ-S properties of the deep northern North Atlantic shifted toward slightly colder (by 0.15°C) and fresher values (by 0.02) (BREWER *et al*, 1983; SWIFT, 1984b). The proximate cause of this deep sea climate change must have been a change in the product water of the Norwegian-Greenland Sea outflows, and from the previous results it is evident that such a change could result from a Θ-S shift of either the source water or the oceanic water. If, as SWIFT (1984b) and LEVITUS (1989) suggest, the NADW Θ-S shift was such as to leave the density unchanged, then so far as this model goes, the resulting Θ and S anomalies would act as passive tracers having no particular significance for outflow dynamics other than the temperature effect upon compressibility.

However, if the density of the source or the oceanic water should change, say because of an uncompensated shift in temperature, then variations of source water density would be expected to affect mainly the volume transport of the product water (rather than its Θ-S) since both of the Norwegian-Greenland Sea outflows are in the range $\Phi \approx 1/2$ where the product water density has only a very weak dependence upon source water density (Sections 2.2.3 and 3.2). For example, to achieve a product water temperature shift of 0.15°C requires either a source water change of 0.5°C, or an oceanic water change of only about 0.2°C. The former has not been observed to our knowledge (but recall the difficulty defining the present Denmark Strait source water, Section 4.1), while the latter is well within the range over which the Labrador and Irminger Sea intermediate waters have been observed to vary (LAZIER, 1988; and compare WÜST, 1935 with the GEOSECS findings).

Given the model's rather acute sensitivity to oceanic conditions, and given the large hydrographic variations known to occur in the Labrador and Irminger Seas, it would appear that a variation in oceanic conditions (rather than marginal sea conditions) is more likely to be a proximate cause of deep Θ-S variations in the North Atlantic. Although these comments are speculative and represent no real progress towards sorting out the origin of the 1970s Θ-S shift, they do serve to emphasize the need to monitor both oceanic and marginal sea conditions if we should ever try to observe how such Θ-S changes might arise in the future.

5. THE FILCHNER ICE SHELF OUTFLOW INTO THE WEDDELL SEA

The main southern hemisphere source of deep and bottom water is the Weddell Sea (WARREN, 1981), where several sites produce dense outflows, including particularly the Filchner Ice Shelf in the southern Weddell Sea (CARMACK and FOSTER, 1975; FOLDVIK, GAMMELSROD and TORRESON, 1985a,b; FOLDVIK, KVINGE and TORRESEN, 1985c). Circulation on the continental shelf brings water which is already very cold into contact with the lower surface of the ice shelf. There the water is modified by melting and may form density-driven plumes on the under side of the ice (NICHOLLS, MAKINSON and ROBINSON, 1991; JENKINS, 1991) and acquires the properties of Ice Shelf Water which has a temperature very near the freezing point, $\Theta = -2.1°C$, and a salinity $S = 34.66$. This source water fills the Filchner Depression, a small basin in the continental shelf, and then spills down the continental slope (FOLDVIK *et al*, 1985a,b) eventually reaching the bottom of the northern Weddell Sea. The outflow of Ice Shelf Water mixes with overlying Warm Deep Water (FOLDVIK *et al*, 1985b) warming it to about $\Theta = -1.5$ to $-0.5°C$ and very slightly increasing its salinity to $S = 34.67$. This product water is called Weddell Sea bottom water[1]. It is joined by other Antarctic outflows (mainly from the Ross Sea, JACOBS, AMOS and BRUCHHAUSEN, 1970) and after some further slow warming, contributes to the Antarctic Bottom Water that covers much of the deep sea floor of the world ocean (REID and LYNN, 1971; GILL, 1973; GRUMBINE, 1991).

5.1 Simulation results

The flow of Ice Shelf Water down the continental slope (see also KILLWORTH, 1977) is simulated by taking as source conditions the Θ and S noted above, which give $\sigma_\theta = 27.94 kg\ m^{-3}$, the lowest of any of the four major outflows studied here. The initial height is 100m, and the current is taken to flow northward out of the Filchner Depression at $0.1 m\ s^{-1}$ (FOLDVIK *et al*, 1985a,b). The initial transport is $1 \times 10^6 m^3 s^{-1}$ giving a width of 100km. The upper 3000m of the oceanic profile is station 32 of FOSTER and CARMACK (1976, Fig.2) observed about 300km northwest of the Filchner Depression, and the deeper portion is taken from data further offshore.

Like the real outflow, the simulated outflow turns northwestward (to the left) very soon after it starts to descend the continental slope (Fig.13a). In the simulation this left turn is a trivial consequence of the sign of the Coriolis parameter; in the Weddell Sea, this left turn may also result from the prevailing clockwise circulation in the Weddell gyre.

Despite the fact that the continental slope is very steep, $\alpha_{max} = 32 \times 10^{-3}$, the outflow currents are fairly small, reaching only about $0.2 m\ s^{-1}$ at maximum and are typically more like $0.1 m\ s^{-1}$ (Fig.14c), which are not inconsistent with current meter observations of this outflow (FOLDVIK *et al*, 1985c; FOSTER and CARMACK, 1976). These comparatively weak currents are a result of the small initial density difference, $0.15 kg\ m^{-3}$. Nevertheless, even a small increase in the current is sufficient to raise the Froude number of the simulated outflow above 1, and there is entrainment of about $1.2 \times 10^6 m^3 s^{-1}$ of Warm Deep Water within a depth range of about 700-1200m. This overlying water is warmer and slightly saltier than the Ice Shelf Water, and its entrainment warms the outflow to about $-0.9°C$, and increases its salinity slightly to about 34.68. These Θ-S values are in the middle of the observed range for Weddell Sea Bottom Water, so that the simulated outflow properties are consistent with those of the actual outflow. The transport of simulated product water, $M_{prd} = 2.2 \times 10^6 m^3 s^{-1}$, appears reasonable, but is poorly known from observations

[1]Deep and bottom water may also be produced within the Weddell Sea by very deep convection coming directly from the sea surface; BERSCH (1988) and GORDON (1978) describe observations of the convective chimneys, and MARTINSON, KILLWORTH and GORDON (1981) develop a model of preconditioning and convection beneath polynyas.

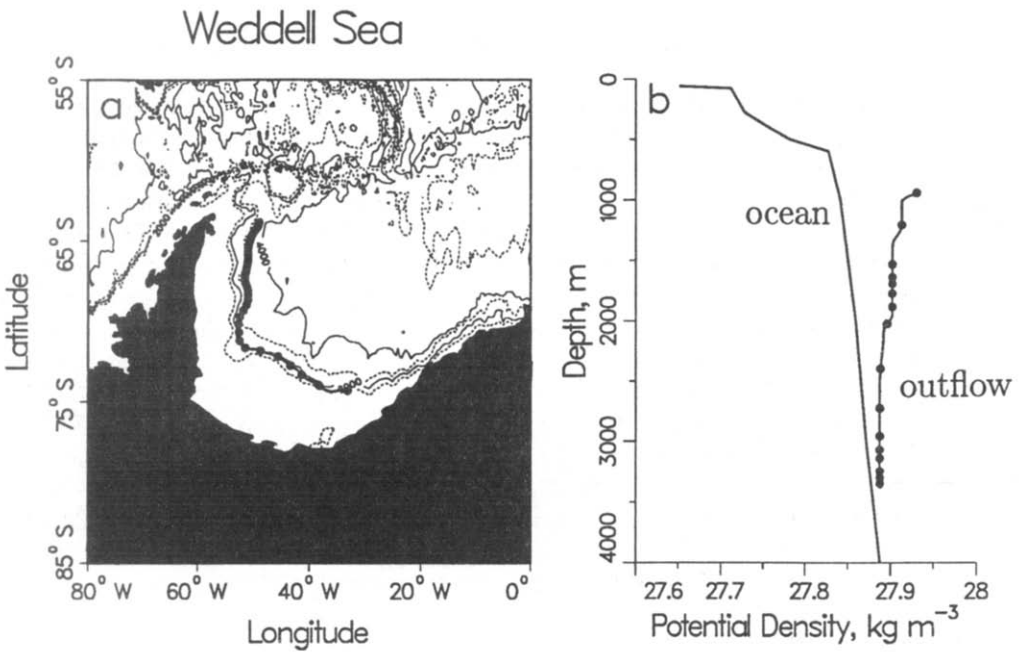

FIG.13. (a) Simulated path of the Filchner Ice Shelf outflow. The outflow is started in the southern Weddell Sea just outside the Filchner Depression and flows northwestward along the continental slope of the southwestern Weddell Sea. Dots are at ten day intervals. (b) Density profiles in the oceanic water (southwestern Weddell Sea) and along the path of the simulated outflow as in Fig.8b.

(FOSTER and CARMACK, 1976). Most of this entrainment occurs soon after the outflow begins its descent of the continental slope, consistent with the inferred site of strongest mixing (FOSTER and CARMACK, 1976).

Despite its small initial density difference with the oceanic water, this outflow continues to the bottom of the Weddell Sea, both because it loses only about 0.03kg m^{-3} of its density as a result of entrainment, and because the deep Weddell Sea is very weakly stratified.

5.2 Numerical experiments; sensitivity to the equation of state and ocean stratification

The use of a full pressure-dependent state equation is especially important in this case because this outflow descends through a very large depth range and is very cold. Since the density difference is almost entirely the result of temperature differences, the pressure-dependence of the *in situ* density is most pronounced (compare Fig.14b with 5b) and causes the *in situ* density difference between the outflow and the surrounding oceanic water to increase as the outflow descends the continental slope (REID and LYNN, 1971; KILLWORTH, 1977). The importance of this thermobaric effect can be checked in the simulation by setting pressure equal to zero in the state equation. This has the effect of reducing the density difference by about 50% when the outflow reaches the deep Weddell Sea (Fig.14b). This is a significant error and reason enough to use a pressure-dependent equation of state. However, the simulated Filchner Ice Shelf outflow reaches the bottom of the Weddell Sea even with this error in place, mainly because the deep Weddell Sea is very weakly stratified (and recall the discussion of Eq.26).

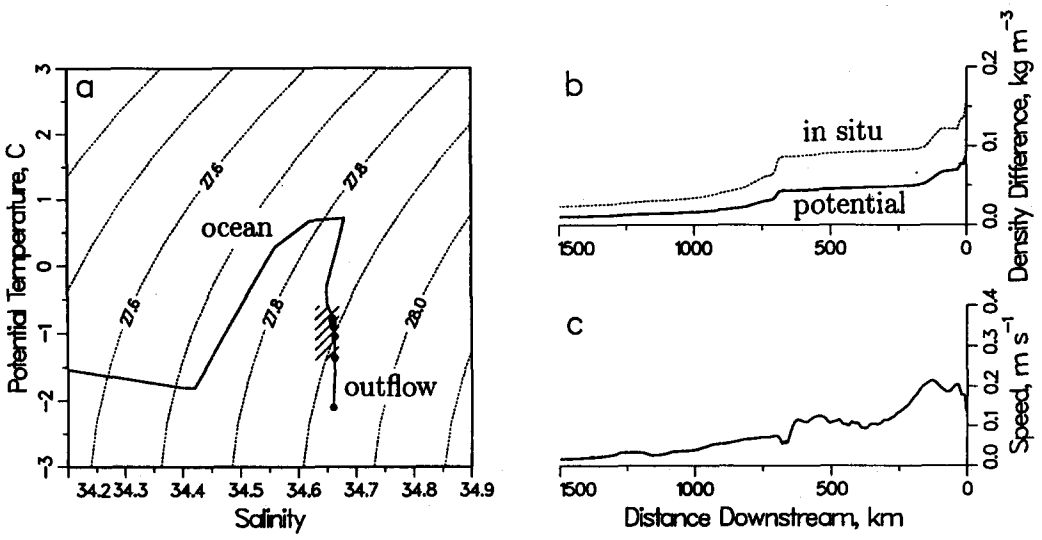

FIG.14. (a) Θ-S diagram for the oceanic profile (southwestern Weddell Sea) and along the path of the simulated Filchner Ice Shelf outflow. The source values for the outflow are -2.1°C and 34.66, and the product water values are within the shaded region which shows the approximate range of Θ-S indicated by GILL (1973) for Weddell Sea Bottom Water. (b) Density difference (outflow minus oceanic) along the path of the simulated outflow. The solid curve is the potential density difference, and the dashed curve is the *in situ* density difference. These differ considerably in this case because of the very cold temperatures of the Filchner Ice Shelf water. (c) Speed along the path of the Filchner Ice Shelf outflow. The geostrophic and simulated speeds are indistinguishable.

The thermobaric effect is just reversed in the case of a salty, warm outflow descending through a colder ocean. This contributes to making the Mediterranean outflow neutrally buoyant at intermediate depths, though its effect on the modern Mediterranean outflow is quite small compared to the effects of entrainment and stratification (Figs 4 and 5).

6. SUMMARY AND REMARKS

A summary of outflow dynamics deduced from the numerical simulations is as follows:

(1) Outflow currents are in a nearly geostrophic balance over most of their path. As a consequence, the external variables that determine the current speed are the density difference, the Coriolis parameter, and the bottom slope. Because of this dominantly geostrophic balance, the initial speed of an outflow is of little consequence, except as it affects the volume transport. Marginal sea outflows thus have the character of density-driven plumes rather than jets.

(2) Bottom stress is crucial to the long-term evolution of an outflow in that it allows an outflow to descend topography without necessarily accelerating. Bottom stress may also allow or cause an outflow current to broaden as it moves downstream.

(3) Strong mixing is generally localized to a region with a large bottom slope, typically the shelf-slope break. Thereafter, unless an even greter slope is encountered downstream, the density difference between the outflow and the surrounding oceanic water is reduced sufficiently that strong entrainment is not likely to happen again. Localized mixing thus appears to be a consequence of the shelf-slope topography underlying most outflows and is not a general property of density currents. This dependence of mixing upon bottom topography is perhaps the distinguishing feature of marginal sea outflows.

(4) Outflows entrain a substantial volume of oceanic water, typically doubling their initial volume transport. Thus the product water of the four major outflows is very roughly half marginal sea source water and half oceanic water. Variations of product water properties may thus arise from changes in either the source water or the oceanic water. Numerical experiments suggest that product water density is most sensitive to changes in the oceanic density, and that the product water transport is equally sensitive to changes in source density or oceanic density.

At the outset of this paper we posed two specific questions to test our understanding of outflows - Why is intense mixing localized? - to which point 3 above is addressed, and - Why do the four major outflows exhibit density reordering? This latter question can be addressed at one of several levels. Considering just the Mediterranean and Denmark Strait outflows, then it is clear from the observations alone that the Mediterranean outflow forms an intermediate water type because its density is decreased by about 1 kg m^{-3} by entrainment of oceanic water having a considerable density difference, initially about 1.5kg m^{-3}. The Denmark Strait outflow descends through an oceanic water mass with which its density contrast is much less, only about 0.4kg m^{-3}. Though the Denmark Strait outflow entrains a significant volume of this water, the resulting density decrease is only about 0.1kg m^{-3}, and hence the Denmark Strait outflow produces bottom water in the northern North Atlantic.

6.1 An accounting of density reordering

To go beyond this qualitative description of the reordering, it is necessary to understand the dependence of the product water densities upon external parameters. To help arrive at this, the simple end-point model has been used to calculate the product water densities of the four outflows already treated by the numerical model. The source water parameters are the same as used in the numerical model and are listed in Table 1. The additional parameters required are the oceanic density, temperature, and salinity at the site where the entrainment occurs, and the bottom depth and bottom slope at that site. These have been read out from the numerical model results, but could probably be picked off a bathymetric chart and an ocean climatology. The only troublesome aspect of this might be the maximum bottom slope, α_{max}, which is generally scale-dependent. In the numerical model the spatial derivative of bottom depth is taken over the scale of the outflow width, which gives a somewhat smoothed representation of the bottom slope.

The results of the end-point model are close to those of the numerical model (Table 1), though not identical. Assuming that product water densities are compared at a depth of 1000m (a depth reached by all four of the outflows), then the end-point model indicates that the Mediterranean outflow produces the least dense product water, while the Filchner Ice Shelf outflow and Denmark Strait outflows are the densest. Thus the end-point model is able to reproduce the density reordering phenomenon.

To see where the variation of product density comes from it is helpful to compare the terms in Eqs 19 and 26:

	σ_{1prd}	=	σ_{1src}	-	$\delta\sigma_1\Phi$	=	σ_{1ocn}	+	$\delta\sigma_1(1-\Phi)$
Med	32.08		32.88		0.80		31.49		0.59
FBC	32.42		32.79		0.36		32.03		0.38
DSt	32.60		32.74		0.16		32.33		0.24
FIS	32.62		32.52		0.08		32.52		0.09
RANGE	0.5	≈	-0.3	-	-0.8	≈	1.0	+	-0.5

where RANGE is just FIS - Med rounded off and $\delta\sigma_1 = \sigma_{1src} - \sigma_{1ocn}$. This tabulation indicates that density reordering results from the entrainment term, which is itself the product of the density difference, which varies by a factor of about 8 (Table 1), and the entrainment magnitude, Φ, which varies by only about 50% over these four cases[1]. Thus the case-to-case variation of the density difference, rather than Φ, appears to account for most of the case-to-case variation of the entrainment term.

A slightly different interpretation comes from examining the terms in Eq.26, where variation of the oceanic density appears to be the single most important factor in setting the product density. The second term, which represents the effect of entrainment, acts to reduce the total range of the product density. While the bottom slope and the Coriolis parameter are very important in the evolution of any particular outflow, it remains that the external parameter which varies the most among the four outflows considered here is the oceanic density. From this view, the Mediterranean outflow produces the least dense product water primarily because it begins at a comparatively shallow depth, ≈ 300m, and in a subtropical ocean. Thus the Mediterranean outflow descends through the least dense oceanic water and for that reason alone it is likely to produce the least dense product water. The other three outflows all begin at greater depths, 600 to 900m, and in polar or subpolar seas where the oceanic water is, of course, somewhat denser. Hence, they produce the densest product waters.

Much like the localized mixing phenomenon noted above, density reordering is a particular result for these four outflows and is not expected to be a general feature of all outflows. What may be general, however, and what is probably the most surprising result of this study, is the apparent greater sensitivity of product water density to variations of the oceanic density (rather than to variations of the source water density) that leads to reordering in these four cases.

[1]It is probably coincidental that these four outflows have nearly equal Φ given the large range in the relevant external variables. For example, the Filchner Ice Shelf outflow has a very small buoyancy flux which increases Φ, but it also has a small geostrophic speed which largely compensates.

6.2 Closing remarks

This analysis is a first approximation to one aspect of the problem of deep water production outlined in Section 1.2. The results given here do not by themselves help us read the paleoceanography record, nor do they help us forecast the deep sea climate. This analysis does indicate some of the physical processes that have to be understood if we are to make progress toward those important goals. Even considering the outflow aspect alone, we can point out three important problems that are worthy of further investigation.

(1) Three-dimensional effects in the local dynamics of outflows. There are several prominent three-dimensional effects evident in the observations of outflows that are either averaged out or ignored in the one-dimensional model. Some of these may produce significant across-stream variations in outflow properties. For example, outflows have a substantial width and are spread out over a sloping bottom so that there is often a substantial across-stream variation in the depth of an outflow. To the extent that the oceanic water column is stratified, then there will be a corresponding across-stream variation in the density difference and thus in the currents. As well, the along-stream thermal wind (geostrophic currents associated with across-stream baroclinic pressure gradients) enhances the buoyancy-driven current on the deeper side of an outflow, and largely cancels it on the shallow side. Both of these three-dimensional effects will lead to across-stream variations of entrainment and thereby to across-stream variations of Θ-S. The Mediterranean outflow produces product water with two modes or cores which appear to arise in this way (BARINGER, 1993; RHEIN and HINRICHSEN, 1993) and the other outflows show substantial Θ-S variability which may have a similar origin (e.g. MANN, 1969, Fig.10). There may also be significant along-stream pressure gradients set up in regions of rapid variation in height or density that are ignored by the present model. Inclusion of these phenomena in an outflow model would perhaps improve the simulations of the Faroe Bank Channel case, and would help connect the analysis of outflows with the comparatively well-developed field of rotating hydraulic flows (PRATT and LUNDBERG, 1991).

(2) Local interactions with the overlying ocean. The strong sensitivity to oceanic conditions calls to question one of our fundamental modelling assumptions, that an outflow can be modelled as a single layer flowing through a resting ocean. In essence, this assumes that the ocean can supply as much water for entrainment as is required, and at no cost. We are not aware that this simplification causes gross errors in the simulation of product water properties. However, by ignoring the ocean's dynamics we are certainly overlooking half of the circulation associated with the outflows. For example, when viewed from the perspective of the North Atlantic Ocean, the Mediterranean outflow and its associated circulation are a source of about $3 \times 10^6 m^3 s^{-1}$ of mixed Mediterranean water (of which roughly one third is 'source water' from the Mediterranean proper). The outflow circulation also acts as a sink for $1 \times 10^6 m^3 s^{-1}$ of surface layer water that enters the Mediterranean, and a sink for another $2 \times 10^6 m^3 s^{-1}$ of upper thermocline water that is entrained by the outflow. The other outflows produce similar sources and sinks which must be an important element of the thermohaline circulation (SPEER and TZIPERMAN, 1990).

(3) Interactions with the general circulation. Since outflow properties set the deep ocean climate, the outflows must interact with one another at climate time scales by way of the deep, general circulation (HOLMEN and ROOTH, 1990; SPEER and TZIPERMAN, 1990). REID (1979) pointed out that any change in the Mediterranean outflow that alters the salinity or volume transport of the product water will eventually change the salinity of the North

Atlantic thermocline and begin a chain of events that, given sufficient time, would change the Norwegian-Greenland Sea outflows and eventually the deep water of the world ocean. A fuller understanding of these global scale aspects of deep water production and circulation is essential if we are to achieve a useful understanding of the ocean as a global conveyor and climate regulator.

7. ACKNOWLEDGEMENTS

This research was sponsored by the US Office of Naval Research through grant numbers N00014-89-J-1053 and N00014-90-J-1474. MOB was supported in part by a Secretary of the Navy Fellowship. We are grateful to Bruce Warren, Joe Reid, Kevin Speer and Harry Bryden for their comments on an earlier draft, and to Barbara Gaffron and Mary Ann Lucas for their help preparing the manuscript. This paper is contribution No.37 of the Gulf of Cadiz Project.

8. REFERENCES

AAGAARD, K., J.H. SWIFT and E.C. CARMACK (1985) Thermohaline circulation in the Arctic Mediterranean seas. *Journal of Geophysical Research*, **90**, 4833-4846.

AMBAR, I. and M.R. HOWE (1979a) Observations of the Mediterranean outflow: I. Mixing in the Mediterranean outflow. *Deep-Sea Research*, **26A**, 535-554.

AMBAR, I. and M.R. HOWE (1979b) Observations of the Mediterranean outflow: II. The deep circulation in the vicinity of the Gulf of Cadiz. *Deep-Sea Research*, **26A**, 555-568.

ARMI, L. and D.M. FARMER (1988) The flow of the Mediterranean water through the Strait of Gibraltar. *Progress in Oceanography*, **21**, 1-105.

BARINGER, M. (1993) *Mixing and dynamics of the Mediterranean outflow*. PhD thesis, Massachusetts Institute of Technology and Woods Hole Oceanographic Institution Joint Program in Oceanography. Cambridge and Woods Hole, Massachusetts. 240pp.

BERSCH, M. (1988) On deep convection in the Weddell Gyre. *Deep-Sea Research*, **35**, 1269-1296.

BORENÄS, K.M. and P.A. LUNDBERG (1988) On the deep-water flow through the Faroe Bank Channel. *Journal of Geophysical Research*, **93**, 1281-1292.

BROECKER, W.S. (1991) The great conveyor. *Oceanography*, **4**, 79-89.

BRASS, G.W., J.R. SOUTHAM and W.H. PETERSON (1982) Warm saline bottom water in the ancient ocean. *Nature*, **296**, 620-623.

BREWER, P.G., W.S. BROECKER, W.J. JENKINS, P.B. RHINES, C.G. ROOTH, J.H. SWIFT, T. TAKAHASHI and R.T. WILLIAMS (1983) A climatic freshening of the deep Atlantic north of 50°N over the past 20 years. *Science*, **222**, 1237-1239.

BRYDEN, H.L. and T.H. KINDER (1991) Recent progress in strait dynamics. *Reviews of Geophysics, Supplement*, 617-631.

BRYDEN, H.L. and H.M. STOMMEL (1982) Origin of the Mediterranean outflow. *Journal of Marine Research*, **40**, 55-71.

BRYDEN, H.L. and H.M. STOMMEL (1984) Limiting processes that determine basic features of the circulation in the Mediterranean Sea. *Oceanologica Acta*, **7**, 289-296.

BRYDEN, H.L., J.C. CANDELA and T.H. KINDER (1994) Exchange through the Strait of Gibraltar. *Progress in Oceanography*, **33**, 201-248.

CARMACK, E.C. and T.D. FOSTER (1975) Circulation and distribution of oceanographic properties near the Filchner Ice Shelf. *Deep-Sea Research*, **22**, 77-90.

COOPER, L.H.N. (1955) Deep water movements in the North Atlantic as a link between climatic changes around Iceland and biological productivity of the English Channel and Celtic Sea. *Journal of Marine Research*, **14**, 347-362.

CREASE, J. (1965) The flow of Norwegian Sea water through the Faroe Bank Channel. *Deep-Sea Research*, **12**, 143-150.

CURRY, W.B., J.C. DUPLESSEY, L.D. LABEYRIE and N.J. SHACKLETON (1988) Changes in the distribution of $\delta^{13}C$ of deep water ΣCO_2 between the last glaciation and the Holocene. *Paleoceanography*, **3**, 317-341.

DICKSON, R.R., E.M. GMITROWICZ and A.J. WATSON (1990) Deep water renewal in the northern North Atlantic. *Nature*, **344**, 848-850.

DUPLESSEY, J.C., N.J. SHACKLETON, R.G. FAIRBANKS, L. LABEYRIE, D. OPPO and N. KALLEL (1988) Deepwater source variations during the last climatic cycle and their impact on the global deepwater circulation. *Paleoceanography*, **3**, 343-360.

ELLISON, T.H. and J.S. TURNER (1959) Turbulent entrainment in stratified flows. *Journal of Fluid Mechanics*, **6**, 423-448.

FOLDVIK, A., T. GAMMELSROD and T. TORRESEN (1985a) Physical oceanography studies in the Weddell Sea during the Norwegian Antarctic Research Expedition 1978/79. *Polar Research*, **3**, 195-207.

FOLDVIK, A., T. GAMMELSROD and T. TORRESEN (1985b) Hydrographic observations from the Weddell Sea during the Norwegian Antarctic Research Expedition 1976/77. *Polar Research*, **3**, 177-193.

FOLDVIK, A., T. KVINGE and T. TORRESEN (1985c) Bottom currents near the continental shelf break in the Weddell Sea. *Oceanology of the Antarctic Continental Shelf, Antarctica Research Series*, **43**, 21-34.

FOSTER, T.D. and E.C. CARMACK (1976) Frontal zone mixing and Antarctic Bottom Water formation in the southern Weddell Sea. *Deep-Sea Research*, **23**, 301-317.

GILL, A.E. (1973) Circulation and bottom water production in the Weddell Sea. *Deep-Sea Research*, **20**, 111-140.

GORDON, A.L. (1978) Deep Antarctic convection west of Maude Rise. *Journal of Physical Oceanography*, **8**, 600-612.

GRANT, A.B. (1968) *Atlas of oceanographic sections*. Report AOL 68-5, Bedford Institute of Oceanography, Dartmouth, Nova Scotia, Canada.

GRIFFITHS, R.W. (1986) Gravity currents in rotating systems. *Annual Review of Fluid Mechanics*, **18**, 59-89.

GRUMBINE, R.W. (1991) A model of the formation of high-salinity shelf water on polar continental shelves. *Journal of Geophysical Research*, **96**, 22049-22062.

HARVEY, J.G. and A. THEODOROU (1986) The circulation of Norwegian Sea overflow water in the eastern North Atlantic. *Oceanologica Acta*, **9**, 393-402.

HEEZEN, B.C. and G.L. JOHNSON (1969) Mediterranean under-current and microphysiography west of Gibraltar. *Bulletin of the Institute of Oceanography, Monaco*, **67**(1382), 1-95.

HOLMEN, K.J. and C.G.H. ROOTH (1990) Ventilation of the Cariaco Trench, a case of multiple source competition? *Deep-Sea Research*, **37**, 203-225.

HOWE, M.R. (1982) The mediterranean water outflow in the Gulf of Cadiz. *Oceanography and Marine Biology, An Annual Review*, **20**, 37-64.

JACOBS, S.S., A.F. AMOS and P.M. BRUCHHAUSEN (1970) Ross Sea oceanography and Antarctic Bottom Water formation. *Deep-Sea Research*, **17**, 935-962.

JENKINS, A. (1991) A one-dimensional model of ice shelf/ocean interaction. *Journal of Geophysical Research*, **96**, 20671-20678.

JOHNSON, G.C. and T.B. SANFORD (1992a) Secondary circulation in the Faroe Bank Channel outflow. *Journal of Physical Oceanography*, **22**, 927-933.

JOHNSON, G.C. and T.B. SANFORD (1992b) Bottom and interfacial stresses on the Mediterranean outflow. Tenth Symposium on Turbulence and Diffusion. Portland, Oregon. *American Meteorological Society*, 105-106.

KENNELLY, M.A., T.B. SANFORD and T.W. LEHMAN (1989) CTD data from the Gulf of Cadiz expedition: R/V *Oceanus* cruise 202. Technical Report APL-UW TR 8917. Applied Physics Laboratory, University of Washington, Seattle. 129pp.

KILLWORTH, P.D. (1977) Mixing on the Weddell Sea continental slope. *Deep-Sea Research*, **24**, 427-448.

KILLWORTH, P.D. (1983) Deep convection in the world ocean. *Reviews of Geophysics and Space Physics*, **21**, 1-26.

LACOMBE, H. (1990) Water, salt, heat and wind in the Med. *Oceanus*, **33**, 26-36.

LAZIER, J.R.N. (1988) Temperature and salinity changes in the deep Labrador Sea, 1962-1986. *Deep-Sea Research*, **35**, 1247-1253.

LEE, A. and D. ELLETT (1965) On the contribution of overflow water from the Norwegian Sea to the hydrographic structure of the North Atlantic Ocean. *Deep-Sea Research*, **12**, 129-142.

LEE, A. and D. ELLETT (1967) On the water masses of the Northwest Atlantic Ocean. *Deep-Sea Research*, **14**, 183-190.

LEVITUS, S. (1989) Interpentadal variability of temperature and salinity in the deep North Atlantic, 1970-1974 versus 1955-1959. *Journal of Geophysical Research*, **94**, 16125-16131.

LIVINGSTON, H.D. (1988) The use of Cs and Sr isotopes as tracers in the Arctic mediterranean seas. *Philosophical Transactions of the Royal Society, London*, **325**, 161-176.

LIVINGSTON, H., J.H. SWIFT and H.G. OSTLUND (1985) Artificial radionuclide tracer supply to the Denmark Strait overflow between 1972 and 1981. *Journal of Geophysical Research*, **90**, 6971-6982.

LYNN, R.J. and J.L. REID (1968) Characteristics and circulation of deep and abyssal waters. *Deep-Sea Research*, **15**, 577-598.

MADELAIN, F. (1970) Influence de la topographie du fond sur l'ecoulment Mediterraneen entre le Detroit de Gibraltar et le Cap Saint-Vincent. *Cahors Oceanographiques.* **22**, 43-61.

MALMBERG, S. (1985) The water masses between Iceland and Greenland. *Rit Fiskideildar, Journal of the Marine Research Institute of Iceland*, **16**, 127-140.

MANN, C.R. (1969) Temperature and salinity characteristics of the Denmark Strait overflow. *Deep-Sea Research*, **16**, 125-137.

MARTINSON, D.G., P.D. KILLWORTH and A.L. GORDON (1981) A convective model for the Weddell Polynya. *Journal of Physical Oceanography*, **11**, 466-488.

MEINCKE, J. (1983) The modern current regime across the Greenland-Scotland Ridge. In *Structure and Development of the Greenland-Scotland Ridge*. M.H.P. BOTT, S. SAKOV, M. TALWANI and J. THIEDE, editors, Plenum Publishing Company, 637-650.

NICHOLLS, K.W., K. MAKINSON and A.V. ROBINSON (1991) Ocean circulation beneath the Ronne ice shelf. *Nature*, **354**, 221-223.

OCHOA, J. and N.A. BRAY (1991) Water mass exchange in the Gulf of Cadiz. *Deep-Sea Research*, **38**, Suppl. 1, 465-503.

PETERSON, W.H. and C.G. ROOTH (1976) Formation and exchange of deep water in the Greenland and Norwegian Seas. *Deep-Sea Research*, **23**, 273-283.

PICKART, R.S. (1992) Water mass components of the North Atlantic deep western boundary current. *Deep-Sea Research*, **39**, 1553-1572.

PRATT, L.J. (1986) Hydraulic control of sill flow with bottom friction. *Journal of Physical Oceanography*, **16**, 1970-1980.

PRATT, L.J. and P.A. LUNDBERG (1991) Hydraulics of rotating strait and sill flow. *Annual Review of Fluid Mechanics*, **23**, 81-106.

PRICE, J.F. (1979) On the scaling of stress-driven entrainment experiments. *Journal of Fluid Mechanics*, **90**, 509-529.

PRICE, J.F., M. O'NEIL BARINGER, R.G. LUECK, G.C. JOHNSON, I. AMBAR, G. PARILLA, A. CANTOS, M.A. KENNELLY and T.B. SANFORD (1993) Mediterranean outflow mixing and dynamics. *Science*, **259**, 1277-1282.

REID, J.L. (1979) On the contribution of the Mediterranean Sea outflow to the Norwegian-Greenland Sea. *Deep-Sea Research*, **26**, 1199-1223.

REID, J.L. and R.J. LYNN (1971) On the influence of the Norwegian-Greenland and Weddell seas upon the bottom waters of the Indian and North Pacific oceans. *Deep-Sea Research*, **18**, 1063-1088.

RHEIN, M. and H.H. HINRICHSEN (1993) Modification of Mediterranean water in the Gulf of Cadiz, studied with hydrographic, nutrient and chlorofluoromethane data. *Deep-Sea Research*, **40**, 267-291.

ROSS, C.K. (1977) Overflow '73 - Denmark Strait, Vol.2: Moored instrument time series. *Bedford Institute of Oceanography Data Series*, BI-D-77-5: 187pp.

ROSS, C.K. (1984) Temperature - salinity characteristics of the 'overflow' water in Denmark Strait during 'OVERFLOW 73'. *Rapport Reunion Conseil international pour l'Exploration de la Mer*, **185**, 111-119.

SAUNDERS, P.M. (1990) Cold outflow from the Faroe Bank Channel. *Journal of Physical Oceanography*, **20**, 29-43.

SIMPSON, J.E. (1987) *Gravity Currents in the Environment and the Laboratory*, Ellis Horwood Ltd., Chichester, 244pp.

SMETHIE, W.M. (1993) Tracing the thermohaline circulation in the western North Atlantic using chlorofluorocarbons. *Progress in Oceanography*, **31**, 51-99.

SMITH, P.C. (1975) A streamtube model for bottom boundary currents in the ocean. *Deep-Sea Research*, **22**, 853-873.

SPEER, K.G. and M.S. MCCARTNEY (1991) Tracing lower North Atlantic Deep Water across the equator. *Journal of Geophysical Research*, **96**, 20443-20448.

SPEER, K. and E. TZIPERMAN (1990) Convection from a source in an ocean basin. *Deep-Sea Research*, **37**, 431-446.

STEELE, J.H., J.R. BARRETT and L.V. WORTHINGTON (1962) Deep currents south of Iceland. *Deep-Sea Research*, **9**, 465-474.

STOMMEL, H.M., H.L. BRYDEN and P. MANGELSDORF (1973) Does the Mediterranean outflow come from great depth? *Pure and Applied Geophysics*, **105**, 879-889.

STULL, R.B. (1988) *An Introduction to Boundary Layer Meteorology*, Kluwer Academic Publishers, Dordrecht, 666pp.

STURGES, W. (1975) Mixing of renewal water flowing into the Caribbean Sea. *Journal of Marine Research*, **33**, Suppl., 117-130.

SWIFT, J.H. (1984a) The circulation of the Denmark Strait and Iceland-Scotland overflow waters in the North Atlantic. *Deep-Sea Research*, **31**, 1339-1355.

SWIFT, J.H. (1984b) A recent Θ-S shift in the deep water of the northern North Atlantic. In: *Climate Processes and Climate Sensitivity*, Geophysical Monograph 29, Maurice Ewing Vol.5, American Geophysical Union, 39-47.

SWIFT, J.H. and K. AAGAARD (1981) Seasonal transitions and water mass formation in the Iceland and Greenland Seas. *Deep-Sea Research*, **28**, 1107-1129.

SWIFT, J.H., K. AAGAARD and S. MALMBERG (1980) The contribution of the Denmark Strait to the deep North Atlantic. *Deep-Sea Research*, **27A**, 29-42.

TALLEY, L.D. and M.S. MCCARTNEY (1982) Distribution and circulation of Labrador Sea water. *Journal of Physical Oceanography*, **12**, 1189-1205.

TURNER, J.S. (1973) *Buoyancy Effects in Fluids*. Cambridge University Press, Cambridge, 368pp.

TURNER, J.S. (1986) Turbulent entrainment: the development of the entrainment assumption and its application to geophysical flows. *Journal of Fluid Mechanics*, **173**, 431-471.

WARREN, B.A. (1981) Deep circulation of the world ocean. In: *Evolution of Phgysical Oceanography, Scientific Surveys in Honor of Henry Stommel*. B.A. WARREN and C. WUNSCH, editors, The MIT Press, Cambridge MA, 6-41.

WHITEHEAD, J.A. (1988) Internal hydraulic control in rotating fluids - applications to oceans. *Geophysical and Astrophysical Fluid Dynamics*, **48**, 169-192.

WHITEHEAD, J.A. (1989) Giant ocean cataracts. *Scientific American*, **260**, 50-57.

WILLEBRAND, J. and J. MEINCKE (1980) Statistical analysis of fluctuations in the Iceland-Scotland frontal zone. *Deep-Sea Research*, **27A**, 1047-1066.

WORTHINGTON, L.V. (1969) An attempt to measure the volume transport of Norwegian Sea overflow water through the Denmark Strait. *Deep-Sea Research*, **16**, 421-432.

WORTHINGTON, L.V. (1975) On the North Atlantic Circulation. *The Johns Hopkins Oceanographic Studies*, **6**, 110pp.

WÜST, G. (1935) The stratosphere of the Atlantic Ocean. W.J. EMERY, editor, 1978, Amerind, New Delhi, 112pp.

ZENK, W. (1975) On the Mediterranean outflow west of Gibraltar. *"Meteor" Forschung Ergebnisse Series A*. **16**, 35-43.

ZENK, W. and L. ARMI (1990) The complex spreading pattern of Mediterranean water off the Portuguese continental slope. *Deep-Sea Research*, **37**, 1805-1823.